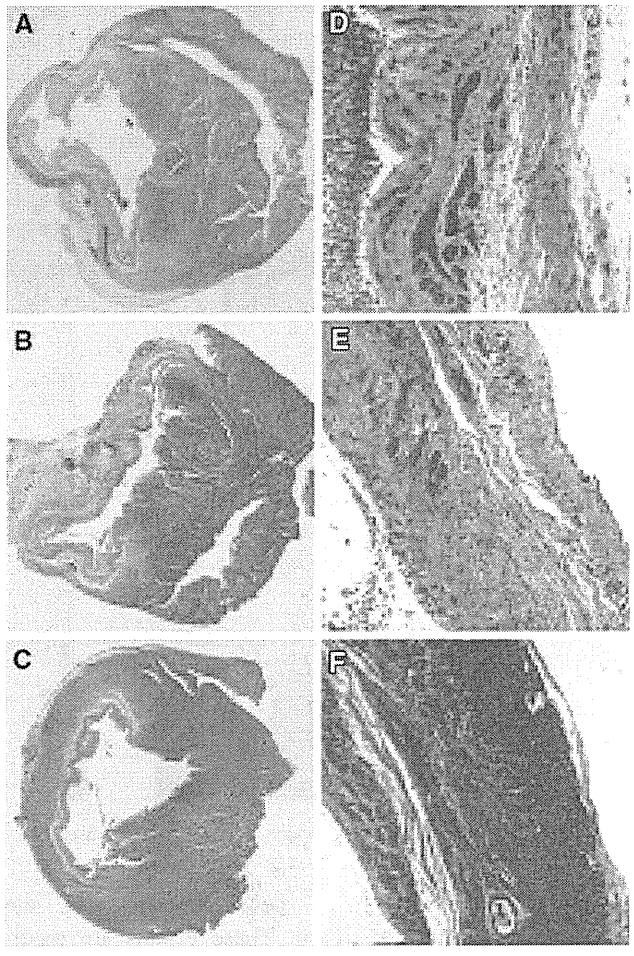

Fig. 3 The gross structure of the heart 4 weeks after treatment was assessed by H&E staining. The sham group (**a**) and the 1-layer group (**b**) showed a large infarcted area in the left ventricular (LV) free wall, but the 3-layer group (**c**) showed a better preserved LV free wall. Interstitial fibrosis 4 weeks after the treatment was assessed by Masson Trichrome staining, which showed more accumulated fibrosis in the sham group (**d**) and the 1-layer group (**e**) than in the 3-layer group (**f**)

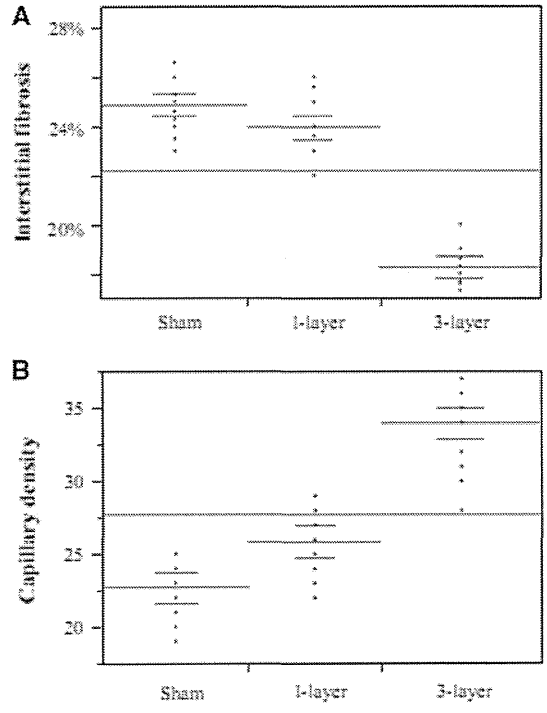

Fig. 4 Masson Trichrome staining revealed a significantly lower percentage of fibrosis 4 weeks after the treatment in the 3-layer group than in the sham or 1-layer groups ($P < 0.05$ vs. the sham and the 1-layer group). Capillary density 4 weeks after treatment, assessed by immunohistochemistry for von Willebrand factor, was significantly greater in the 3-layer group than in the sham or 1-layer groups ($P < 0.05$ vs. the sham and the 1-layer group)

cell-sheet might be a critical limiting factor to the effects. In fact, it was reported that ischemia-related cell-necrosis occurs in the transplanted cells in accordance with the number of cell-sheets filled up [10, 17]. Furthermore, our researchers reported previously that the therapeutic effects of skeletal myoblast cell-sheets increased with the number of layers, but plateaued at five layers, possibly because of ischemia-related functional impairment of the transplanted cell-sheet, although skeletal myoblasts are known to be highly resistant to ischemic stimuli [10, 18, 19]. This study showed that the therapeutic effects of the CSC cell-sheet increased up until three layers, despite poor vascular support after acute infarction of the cell-sheet transplanted area, warranting 3-layered CSC cell-sheet transplantation for treating ischemia-related cardiac failure. Integration of the transplanted CSC cell-sheet into the native myocardium is also a concern of this treatment, as the cell-sheet was simply attached to the epicardial surface. However, this study unveiled that the transplanted cells migrated into the native myocardium and differentiated to heart-composing cells, although the biological mechanisms of this migration process remain unclear.

This study is limited by fact that we used a rodent model transplanted with cells of human origin. The difference in factors related to biological actions between the rat and the human might have modulated the therapeutic effects of this treatment, although a number of previous reports would justify using this model to mimic the clinical scenario [17, 20]. Moreover, using the cells from one patient in the in vivo study might not be appropriate to investigate the effects of CSC of human origin in general, although the cellular behavior did not seem to differ among more than five patients in vitro (data not shown), in accordance with previous reports [21].

In conclusions, the 3-layered cell-sheet improved cardiac function associated with angiogenic and anti-fibrotic effects in a rat model. Thus, the delivery of a sufficient number of CSCs by a cell-sheet method represents a promising treatment for cardiac failure, although further optimization is essential.

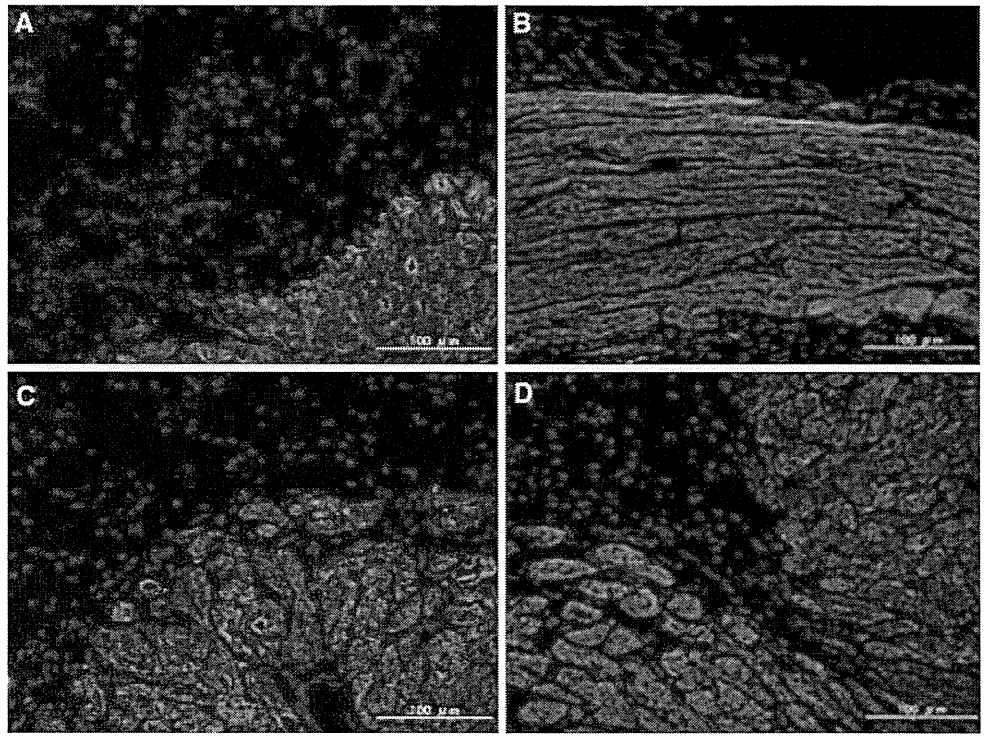

Fig. 5 The presence and distribution of transplanted CSCs of human origin were immunohistologically assessed using human-specific anti-HLA antibody. By 4 weeks after transplantation, the 3-layer group showed abundant human-specific HLA-positive transplanted cells in tissues that were epicardially attached to the native cardiac tissue (**a**). Some human-specific HLA-positive transplanted cells were present in the interstitium of the native myocardium (**b–d**)

Conflict of interest There are no relationships or conflicts of interest related to this manuscript.

References

1. Braunwald E, Bristow M. Congestive heart failure: fifty years of progress. Circulation. 2000;102:14–23.
2. Kania G, Boheler KR, Landmesser U, Wojakowski W. Stem cells in heart failure. Stem Cells Int. 2011 [Epub Nov30].
3. Robey TE, Saiget MK, Reinecke H, Murry CE. Systems approaches to preventing transplanted cell death in cardiac repair. J Mol Cell Cardiol. 2008;45:567–81.
4. Giraud MN, Armbruster C, Carrel T, Tevaearai HT. Current state of the art in myocardial tissue engineering. Tissue Eng. 2007;13:1825–36.
5. Jawad H, Ali NN, Lyon AR, Chen QZ, Harding SE, Boccaccini AR. Myocardial tissue engineering. Br Med Bull. 2008;87:31–47.
6. Beltrami AP, Barlucchi L, Torella D, Baker M, Limana F, Chimenti S, et al. Adult cardiac stem cells are multipotent and support myocardial regeneration. Cell. 2003;114:763–76.
7. Shimizu T, Yamato M, Kikuchi A, Okano T, et al. Two-dimensional manipulation of cardiac myocyte sheets utilizing temperature-responsive culture dishes augments the pulsatile amplitude. Tissue Eng. 2001;7:141–51.
8. Sawa Y, Miyagawa S, Sakaguchi T, Fujita T, Matsuyama A, Saito A, Shimizu T, Okano T. Tissue engineered myoblast sheets improved cardiac function sufficiently to discontinue LVAS in a patient with DCM: report of a case. Surg Today. 2012;42:181–4.
9. Shimizu T, Yamato M, Kikuchi A, Okano T. Cell sheet engineering for myocardial tissue reconstruction. Biomaterials. 2003;24:2309–16.
10. Sekiya N, Matsumiya G, Miyagawa S, Saito A, Shimizu T, Okano T, et al. Layered implantation of myoblast sheets attenuates adverse cardiac remodeling of the infarcted heart. J Thorac Cardiovasc Surg. 2009;138:985–93.
11. Imanishi Y, Miyagawa S, Maeda N, Fukushima S, Kitagawa-Sakakida S, Daimon T, et al. Induced adipocyte cell-sheet ameliorates cardiac dysfunction in a mouse myocardial infarction model: a novel drug delivery system for heart failure. Circulation. 2011;124:S10–7.
12. Zakharova L, Mastroeni D, Mutlu N, Molina M, Goldman S, Diethrich E, et al. Transplantation of cardiac progenitor cell sheet onto infarcted heart promotes cardiogenesis and improves function. Cardiovasc Res. 2010;87:40–9.
13. Forte E, Chimenti I, Barile L, Gaetani R, Angelini F, Ionta V, et al. Cardiac cell therapy: the next (re)generation. Stem Cell Rev. 2011;7:1018–30.
14. Tongers J, Losordo DW, Landmesser U. Stem and progenitor cell-based therapy in ischaemic heart disease: promise, uncertainties, and challenges. Eur Heart J. 2011;32:1197–206.
15. Kawaguchi N, Smith AJ, Waring CD, Hasan MK, Miyamoto S, Matsuoka R, et al. c-kitpos GATA-4 high rat cardiac stem cells foster adult cardiomyocyte survival through IGF-1 paracrine signaling. PLoS ONE. 2010;5:e14297.
16. Rota M, Padin-Iruegas ME, Misao Y, De Angelis A, Maestroni S, Ferreira-Martins J, et al. Local activation or implantation of cardiac progenitor cells rescues scarred infarcted myocardium improving cardiac function. Circ Res. 2008;103:107–16.
17. Shudo Y, Miyagawa S, Fukushima S, Saito A, Shimizu T, Okano T, et al. Novel regenerative therapy using cell-sheet covered with omentum flap delivers a huge number of cells in a porcine myocardial infarction model. J Thorac Cardiovasc Surg. 2011;142:1188–96.
18. Hata H, Matsumiya G, Miyagawa S, Kondoh H, Kawaguchi N, Matsuura N, et al. Grafted skeletal myoblast sheets attenuate myocardial remodeling in pacing-induced canine heart failure model. J Thorac Cardiovasc Surg. 2006;132:918–24.
19. Memon I, Sawa Y, Fukushima N, Matsumiya G, Miyagawa S, Taketani S, et al. Repair of impaired myocardium by means of implantation of engineered autologous myoblast sheets. J Thorac Cardiovasc Surg. 2005;130:1333–41.

20. Tang Y. Cellular therapy with autologous skeletal myoblasts for ischemic heart disease and heart failure. Methods Mol Med. 2005;112:193–204.

21. He J, Vu D, Hunt G, Chugh A, Bhatnagar A, Bolli R. Human cardiac stem cells isolated from atrial appendages stably express c-kit. PLoS ONE. 2011;6:e27719.

Circulation Journal
Official Journal of the Japanese Circulation Society
http://www.j-circ.or.jp

ORIGINAL ARTICLE
Regenerative Medicine

Human Cardiac Stem Cells With Reduced Notch Signaling Show Enhanced Therapeutic Potential in a Rat Acute Infarction Model

Takenori Matsuda; Shigeru Miyagawa, MD, PhD; Satsuki Fukushima, MD, PhD; Satoru Kitagawa-Sakakida, MD, PhD; Hiroshi Akimaru, PhD; Miki Horii-Komatsu, BSc; Atsuhiko Kawamoto, MD, PhD; Atsuhiro Saito, PhD; Takayuki Asahara, MD, PhD; Yoshiki Sawa, MD, PhD

Background: Because human cardiac stem cells (CSC) have regeneration potential in damaged cardiac tissue, there is increasing interest in using them in cell-based therapies for cardiac failure. However, culture conditions, by which CSCs are expanded while maintaining their therapeutic potential, have not been optimized. We hypothesized that the plating cell-density would affect proliferation activity, differentiation and therapeutic potential of CSCs through the Notch signaling pathway.

Methods and Results: Human CSCs were plated at 4 different densities. The population doubling time, C-KIT positivity, and dexamethasone-induced multidifferentiation potential were examined in vitro. The therapeutic potential of CSCs was assessed by transplanting them into a rat acute myocardial infarction (AMI) model. The low plating density (340 cells/cm^2) maintained the multidifferentiation potential with greater proliferation activity and C-KIT positivity in vitro. On the other hand, the high plating density (5,500 cells/cm^2) induced autonomous differentiation into endothelial cells by activating Notch signaling in vitro. CSCs cultured at low or high density with Notch signal inhibitor showed significantly greater therapeutic potential in vivo compared with those cultured at high density.

Conclusions: CSCs cultured with reduced Notch signaling showed better cardiomyogenic differentiation and therapeutic potentials in a rat AMI model. Thus, reducing Notch signaling is important when culturing CSCs for clinical applications. (*Circ J* 2014; **78:** 222–231)

Key Words: Cardiac stem cells; Cell culture; Notch signaling

Cardiac failure is a major cause of reduced quality of life and mortality.[1,2] Although cardiac tissue is known to have limited regeneration capacity, it has been shown that damaged cardiac tissue is regenerated by cardiac stem cells (CSCs), which are identified as C-KIT-positive cells in the heart,[3] through their proliferation and differentiation into functional cardiomyocytes, vascular smooth muscle cells, and vascular endothelial cells (ECs), and through release of a variety of factors that activate native healing processes.[4] Although transplantation of autologous stem cells into the heart has been proven to enhance this regenerative capacity of the damaged heart,[5] transplantation of CSCs that have been expanded in vitro may have promise in maximizing the regeneration process.[6] The magnitude of the therapeutic effect of CSC transplantation is determined by the cell preparation and delivery method, though the protocol for preparing CSCs has not been fully established.[7] Determination of the culturing protocol will be critical for the clinical application of patient-derived CSCs that may be isolated from limited biopsy samples.

Editorial p69

The cell preparation protocol of CSCs involves multiple steps, including enzymatic digestion of tissues, cell isolation, and cultivation, that will affect the fundamental behavior and therapeutic potential of CSCs.[8,9] Although the cell isolation protocol has been intensively studied,[3,10–13] the cell cultivation protocol has not. Among the many parameters of the culture

Received April 24, 2013; revised manuscript received July 20, 2013; accepted August 20, 2013; released online October 9, 2013 Time for primary review: 22 days

Department of Cardiovascular Surgery, Osaka University Graduate School of Medicine, Suita (T.M., S.M., S.F., S.K.-S., Y.S.); Vascular Regeneration Research Group, Institute of Biomedical Research and Innovation, Kobe (T.M., H.A., M.H.-K., A.K., T.A.); Medical Center for Translational Research, Osaka University Hospital, Suita (A.S., Y.S.); and Department of Regenerative Medicine Science, Tokai University School of Medicine, Isehara (T.A.), Japan.

Mailing address: Professor Yoshiki Sawa, MD, PhD, Department of Cardiovascular Surgery, Osaka University Graduate School of Medicine, 2-2 Yamadaoka, Suita 565-0871, Japan. E-mail: sawa-p@surg1.med.osaka-u.ac.jp

ISSN-1346-9843 doi:10.1253/circj.CJ-13-0534

conditions, it has been suggested that cell density at plating modulates fundamental behavior of stem cells such as proliferation and differentiation, indicating that the plating density may affect the therapeutic potential of CSCs.[14,15] In addition, it was reported that Notch signaling in direct cell-cell communication may be associated with fundamental behavior of cells under cultivation, including the lineage specification of cardiac progenitor cells.[16–18] We hypothesized that the plating cell-density would affect proliferation activity, differentiation and therapeutic potential of human CSCs by regulating Notch signaling, with the aim of exploring the optimal CSC cultivation protocol for treating cardiac failure.

Methods

Isolation and Cultivation of CSCs

All procedures were in accordance with the ethical standards of the institutional committee on human experimentation (control number: 729-4). CSCs were isolated from the right atrium of 3 patients with dilated cardiomyopathy (12–55 years old; data from the 12-year-old patient are mainly used in this report). In short, the cells were separated from the tissue by enzymatic digestion [37°C with 1 mg/ml of collagenase (17454, Serva Electrophoresis, Heidelberg, Germany) in Ham's F12 medium] after dissecting fat and fibrous tissues and mincing. The digestion was performed for a total of 5 reactions (60 rpm×20 min/reaction, 8 ml/reaction in 50 ml tube) then overnight digestion (for 12 h) was performed for the remaining debris with 0.1 mg/ml of collagenase solution (37°C, 60 rpm, 10 ml in 50 ml tube). After each reaction, the supernatant was collected and then the cells were collected by centrifugation (4°C, 500 g, 5 min) and plated on a normal 10-cm culture dish (353003, BD Biosciences, Franklin Lakes, NJ, USA) with complete medium [Ham's F12 medium supplemented with 10% fetal bovine serum (FBS; SH30406.02, Hyclone, Thermo Fisher Scientific, Waltham, MA, USA), 5 mU/ml human erythropoietin (E5627-10UN, Sigma-Aldrich, St. Louis, MO, USA), 10 ng/ml basic fibroblast growth factor (100-18B, PeproTech, Rocky Hill, USA), 0.2 mmol/L L-glutathione (G6013, Sigma-Aldrich) with antibiotics].[6] The medium was changed on day 2. On day 5, the cells were collected with trypsin (T3924, Sigma-Aldrich) and replated on 10-cm dishes at 170 cells/cm^2. At the second passage (P1), the cells were collected with non-enzymatic solution (C5914, Sigma-Aldrich), labeled with anti-C-KIT antibody (130-091-735, Miltenyi Biotec, Bergisch Gladbach, Germany) followed by FcR blocking reagent (130-059-901, Miltenyi Biotec) in 3% FBS/PBS, and subjected to FACS (FACS Aria, BD Biosciences) to isolate the CSCs. As the negative control sample, mouse IgG1-phycoerythrin (130-092-212, Miltenyi Biotec) was used. The dead cells were excluded from the sample by using 7AAD (559925, BD Biosciences). After sorting, the CSCs were passaged (340 cells/cm^2) every 5 days. At P5, CSCs were sorted again as described. The purified CSCs were plated on normal culture dishes at different densities with and without 100 nmol/L of gamma secretase inhibitor XXI (GSI; Merck, Darmstadt, Germany)[16] and passaged every 5 days.

qPCR

Total RNA was extracted using an RNeasy mini kit (Qiagen, Hilden, Germany) with on-column DNase digestion (RNase-Free DNase set, Qiagen). The extracted RNA was subjected to reverse transcription (Omniscript reverse transcriptase, Qiagen) with random primers (Invitrogen-Life Technologies, Carlsbad, CA, USA). qPCR (quantitative real-time PCR) was performed using predesigned TaqMan primers/probes [assay ID; GAPDH: Hs99999905_m1, P21: Hs00355782_m1, P53: Hs01034249_m1, ETS1: Hs00901425_m1, TIE2: Hs00945155_m1, HES1: Hs00172878_m1, C-KIT: Hs00174029_m1, IL8: Hs99999034_m1, VEGFA: Hs00900055_m1, cTnT: Hs00165960_m1, PDGFRB: Hs01019589_m1, HGF: Hs00900070_m1, Applied Biosystems-Life Technologies, Carlsbad, CA, USA] and a 7500 Fast real-time PCR system (Applied Biosystems). GAPDH was used as the internal control.

Tube Formation Assay

CSCs in EBM2 (CC-3156, Lonza, Basel, Switzerland) supplemented with 0.2% FBS were plated onto a Matrigel (BD Biosciences) -coated 96-well plates (7.5×10^3 cells per well) and incubated for 16 h.[19] Subsequently, the total tube length per well was measured[20] by analytic software (BZII, Keyence, Osaka, Japan).

Immunocytofluorescence Analysis of Cell Differentiation

αMEM supplemented with 10% FBS and 10^{-8} mol/L dexamethasone was used to induce differentiation of CSCs.[3] In short, CSCs were replated (3,400 cells/cm^2) onto a cover slip coated with 0.1% gelatin and incubated under 5% CO_2 at 37°C for 7 days. The cells were fixed with 4% paraformaldehyde and labeled with primary antibodies against αSA (alpha sarcomeric actin, A2172, Sigma-Aldrich), anti-αSMA (alpha smooth muscle actin, A2574, Sigma-Aldrich), or anti-TIE2 (T6577, Sigma-Aldrich). The samples were visualized with appropriate secondary antibodies and counterstained with DAPI.

Rat Acute Myocardial Infarction (AMI) Model and Cell Transplantation

The animal study protocols were approved by the Animal Care and Use Committee of the Osaka University (21-030-2). The left coronary artery (LCA) was permanently ligated in nude rats (F344/NJcl-rnu/rnu, 8-week-old females, CLEA Japan, Tokyo, Japan) under inhalation anesthesia with 2.0% isoflurane through endotracheal intubation.[21] Immediately after the ligation, 8×10^4 cells[3] or 3×10^6 cells (for immunostaining against HNA/MLC and qPCR for VEGFA/HGF (Hepatocyte growth factor)) per rat were transplanted by intramuscular injection into the infarct's border zone.

Transthoracic Echocardiography (TTE)

TTE was performed under inhalation anesthesia with 1.5% isoflurane as described previously.[21]

Histological Examination

Rat hearts were collected after retrograde infusion of phosphate-buffered saline (PBS) supplemented with 50 mmol/L potassium chloride and 100 units/ml heparin. The hearts were embedded in OCT (Sakura Finetek Japan, Tokyo, Japan), cut into 5-μm sections, and fixed with 4% paraformaldehyde.[22] The sections were then stained with Masson's trichrome or immunohistologically against von Willebrand factor (vWF; A0082, Dako, Glostrup, Denmark), HNA (human nuclear antigen, MAB1281, Millipore, MA, USA), or MLC (myosin light chain, ab79935, Abcam, MA, USA) by similar methods to those mentioned earlier.

To calculate the percentage of left ventricle (LV) that was fibrotic, the total LV and fibrotic areas (blue-colored) were traced and measured using analytical software (BZII, Keyence). The percentage of MLC-positive cells was calculated as the number of HNA and MLC double-positive cells divided by the number of HNA-positive cells in a high-power magnification area (×200).

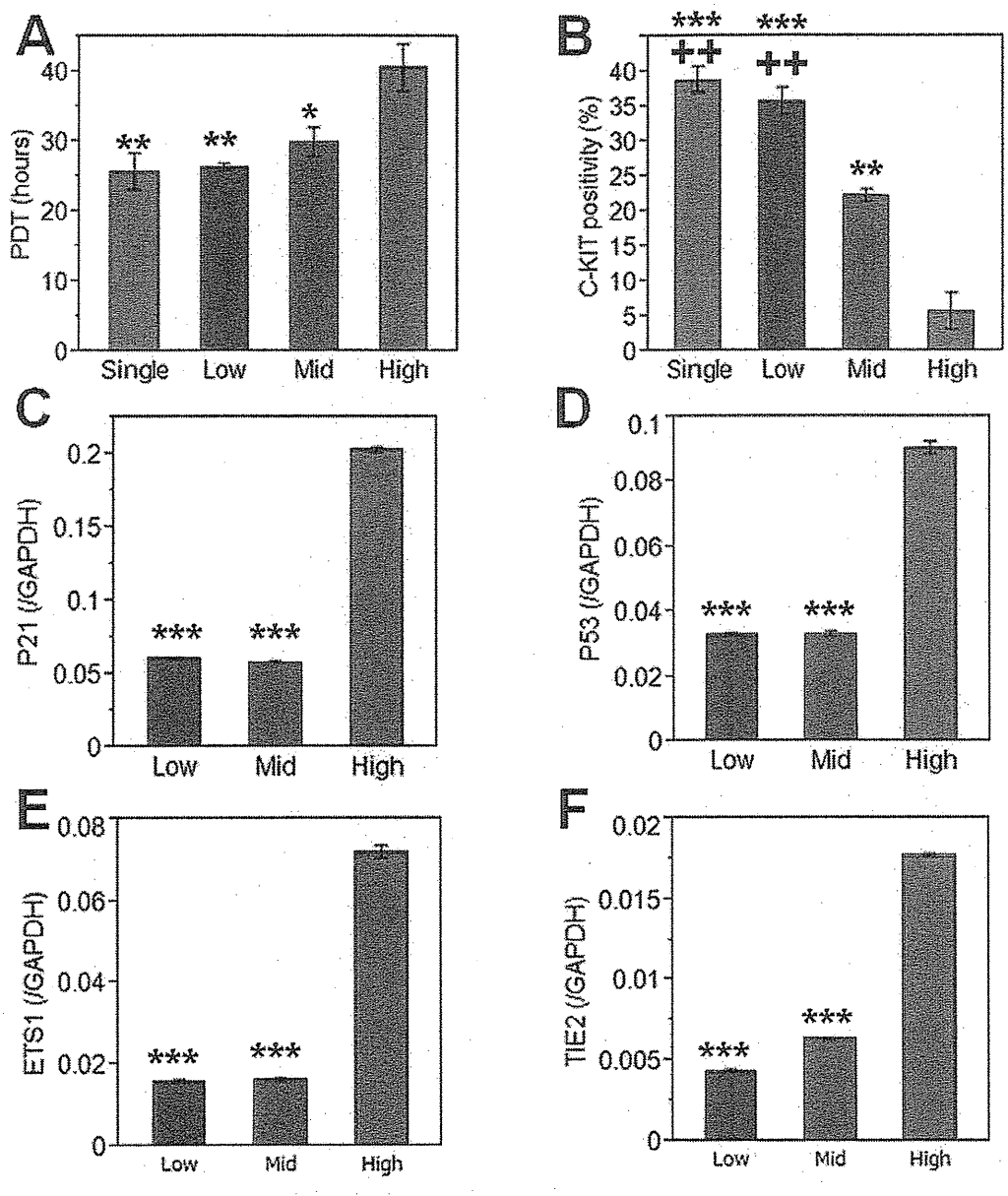

Figure 1. Population doubling time (PDT) and C-KIT positivity in cardiac stem cells. (**A**) PDT was averaged for 3 passages. (**B**) C-KIT positivity was assessed by FACS and averaged for 3 passages. (**C–F**) qPCR analysis. The values are the average for triplicate in a representative experiment. *P<0.05, **P<0.01, ***P<0.0001 vs. "High" group. ++P<0.01 vs. "Mid" group.

Statistical Analysis

All data represent the mean±SEM. Statistical analyses were performed using software (JMP9, SAS Institute Japan, Tokyo, Japan or Prism 5, GraphPad Software, La Jolla, CA, USA). For multiple comparisons, ANOVA with Tukey's HSD post-hoc test was used. For the qPCR analysis of C-KIT, interleukin (IL)-8, and VEGF (Vascular endothelial growth factor) A, the raw data (normalized by GAPDH) of the "High" or "High+GSI" group were normalized to the data of the "Low" group from the same patient, because samples from 3 different patients were used for this experiment, and 1-sample t-test (vs. Low group) or unpaired t-test (High vs. High+GSI group) was used. For echocardiography, the delta values (the difference between before and 3 weeks after the transplantation) were used. If the P-value was <0.05, the difference was considered significant.

Results

Plating Density-Dependent Proliferation Activity and Purity of CSCs

Based on previous reports, we hypothesized that the plating density would affect the proliferation activity and purity of CSCs. We expected that higher plating density would increase Notch signaling, induce differentiation and therefore decrease the proliferation activity and purity of CSCs. To examine this, we isolated CSCs from samples (eg, 5.6×10^5 cells/g muscle at P1). After several passages of culture, we purified C-KIT pos-

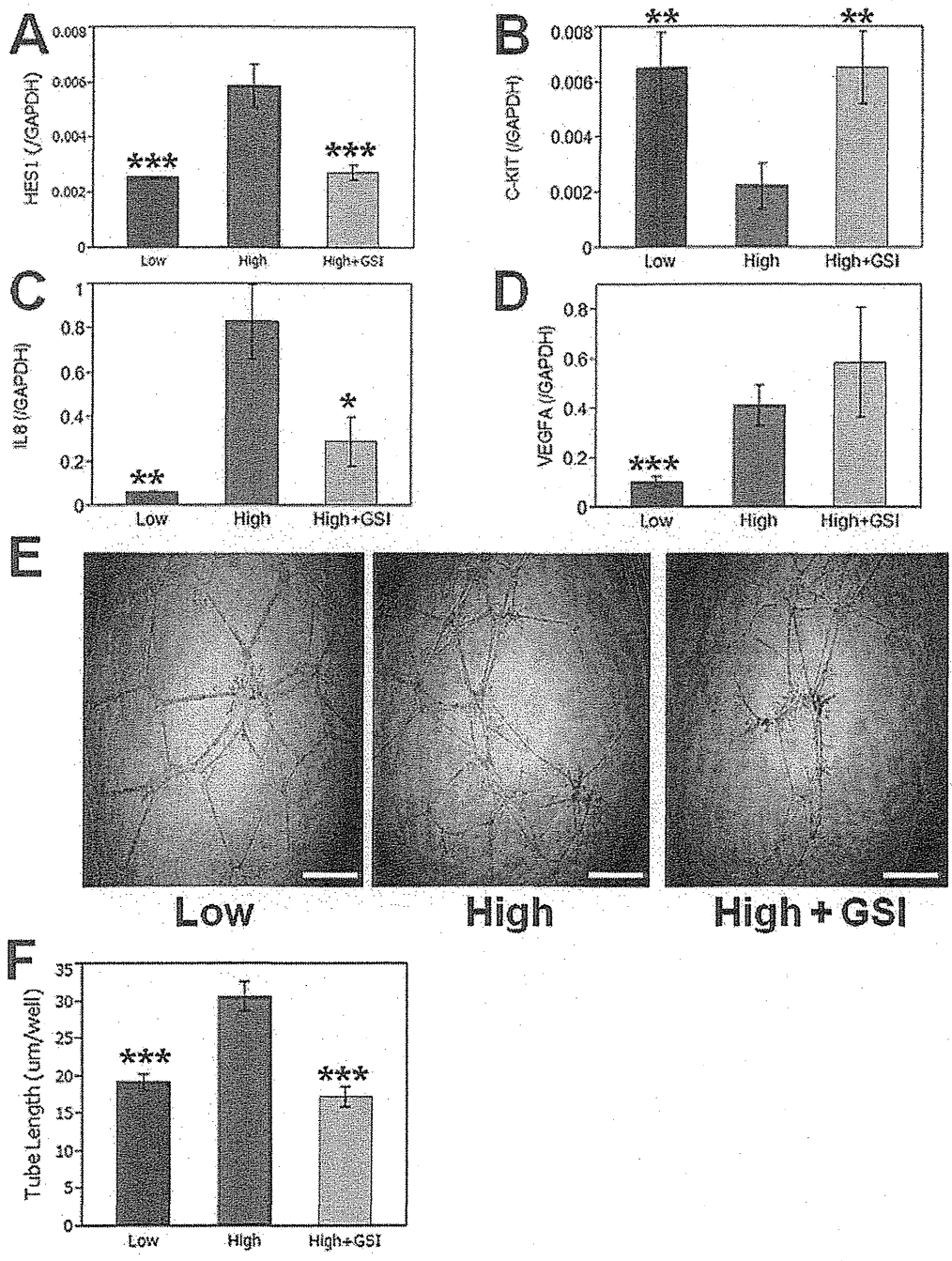

Figure 2. Vascular endothelial cell (EC)differentiation of cardiac stem cells resulting from high-density culture through Notch signaling activation. (**A–D**) qPCR analysis was performed after 3 passages under each plating density condition for the target gene of Notch signaling (*HES1*), C-KIT, and EC-related genes (IL-8 and VEGFA). (**E**) Representative morphologies of tube formation assay are shown. Original magnification, ×20. Scale bars=500μm. (**F**) Quantitative analysis of the tube formation assay. The total length of tubes per well was measured. The results from 12–14 wells per group were analyzed. *P<0.05, **P<0.01, ***P<0.0001 vs. "High" group.

itive cells by FACS (93.0±0.3%; mean±SEM) and plated at different densities (cells/cm^2): 86 (Single), 340 (Low), 1,400 (Mid), or 5,500 (High).

The proliferation activity of CSCs in relation to plating density was assessed by population doubling time (PDT), which was measured at each passage until the 3rd passage and then averaged (**Figure 1A**). The Single, Low and Mid groups showed a significantly shorter PDT than the High group. Purity of CSCs in relation to plating density was assessed by C-KIT positivity, which was measured at each passage until the 3rd passage and then averaged (**Figure 1B**). The Single and Low groups showed significantly greater C-KIT positivity than

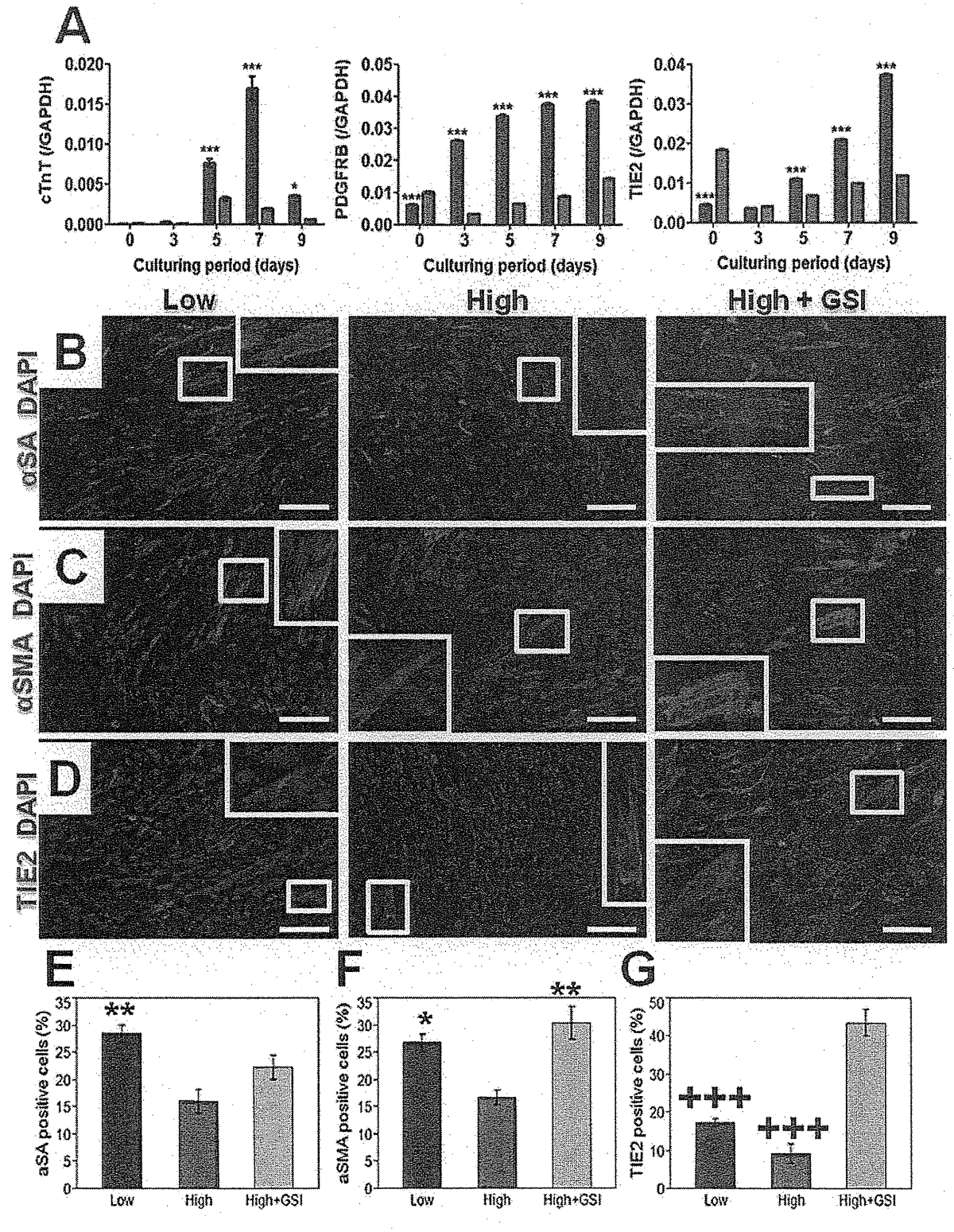

Figure 3. Differentiation potentials of cardiac stem cells (CSC) in vitro. (**A**) CSCs cultured at a low (blue) or high (red) plating density were incubated with dexamethasone for 9 days. The expression levels of cardiomyocyte (cTnT), smooth muscle cell (PDGFRB), and endothelial cell (TIE2) markers were analyzed by qPCR during the culture period. (**B–D**) Immunostaining for differentiated cells on day 7. Scale bars=100 μm. (**E–G**) Quantitative analysis of the immunostaining. The results from 11–20 fields per group were examined. *P<0.05, **P<0.01 vs. "High" group. +++P<0.0001 vs. "High+GSI" group.

the Mid and High groups, and the Mid group showed significantly greater C-KIT positivity than the High group. These findings suggested that lower plating cell densities might contribute to preservation of the proliferation activity and purity of CSCs in vitro.

Plating Density-Dependent Transcriptional Profiles of CSCs

Cellular function of CSCs in relation to the plating cell-density and Notch signaling was further assessed by qPCR for cell-cycle regulating genes (P21 and P53), EC markers (ETS1, TIE2, IL8, and VEGFA), Notch-signaling target gene (*HES1*)[23] and C-KIT. Expression of these genes in CSCs was analyzed in the Low, Mid and High groups. In addition, GSI, which is a known Notch signal inhibitor,[16,17,24,25] was added to the culture medium of the High group to investigate the influence of Notch signaling on the gene expression.

The Low and Mid groups showed significantly lower levels of expression of P21, P53, ETS1, and TIE2, compared with the High group (**Figures 1C–F**). In addition, the Low group showed lower expressions of HES1, IL8 and VEGFA than the High group, and C-KIT expression was significantly greater in the Low group than in the High group (**Figures 2A–D**). Of note, the addition of GSI in the High group diminished the expression of HES1 and IL-8, but not of VEGFA. In addition, C-KIT expression in the High group was restored to that of the Low group by GSI treatment (**Figure 2B**). These findings suggested that higher plating densities might induce endothelial differentiation followed by termination of cell cycles, which slows PDT and diminishes the level of expression of C-KIT through Notch signal activation.

Plating density-dependent EC differentiation of CSCs in relation to Notch signaling was further assessed by the tube formation assay on Matrigel in vitro. Consistent with EC marker expression, the High group generated longer tubes than the Low group. Notably, GSI treatment diminished the tube formation activity in the High group to the level of the Low group, indicating active involvement of Notch signaling in the plating density-dependent EC differentiation of CSCs in vitro (**Figures 2E–F**).

Retained Multipotency in CSCs Under Low-Density Culture

Because we confirmed that a higher plating density might induce EC differentiation of CSCs, we next examined the multipotency of CSCs in relation to the plating density by inducing differentiation in vitro. We expected CSCs at a lower plating density to maintain multipotency, and conversely, lose multipotency at a higher plating density. CSCs that were cultured in Low and High conditions were replated with dexamethasone and incubated for 9 days.[3,26,27] Expressions of cTnT (cardiomyocyte marker), PDGFRB (SMC marker), and TIE2 in each group were serially assessed by qPCR. cTnT, PDGFRB, and TIE2 were all upregulated in Low group over the culture period compared with the High group (**Figure 3A**), suggesting that CSCs cultured at low density may retain greater multipotency than those cultured under High conditions.

The differentiation potential of CSCs was further assessed by immunostaining for αSA (cardiomyocyte marker), αSMA (SMC marker) and TIE2 on day 7 (**Figures 3B–D**). The number of αSA- or αSMA-positive cells was significantly greater in the Low group than in the High group, and the TIE2-positive cell number tended to be greater in the Low group than in the High group (**Figures 3E–G**). Of note, the cells cultured under High conditions with GSI showed a significantly greater positivity for αSMA and TIE2 than those under pure High culture conditions, though GSI treatment did not affect significantly αSA positivity. These findings suggested that the multipotency of CSCs was hampered by higher plating density through Notch signaling-mediated EC differentiation.

Therapeutic Effects of CSCs in a Rat AMI Model

Our in vitro data suggested that CSCs at a lower plating density maintained multipotency. Because multipotency may be required for their therapeutic potential, we next examined this in relation to the plating density and Notch signaling by transplanting CSCs into a rat AMI model.[3] We expected CSCs cultured under Low and High+GSI conditions to have greater therapeutic potential than those under High conditions. CSCs that were prepared in Low, High, or High+GSI culture conditions suspended with PBS or PBS only were injected into the infarct-border zone just after permanent ligation of the LCA. Effects of the CSC-transplantation therapy were assessed by standard TTE.

TTE revealed that all groups consistently showed progressive enlargement of the end-diastolic volume of the LV. However, the Low group showed significantly less progressive enlargement in the end-systolic volume of the LV and significantly less progressive reduction in LV ejection fraction compared with the High group, which showed a similar trend to the PBS-only group (**Figures 4A–C**). Notably, the enlarged LV end-systolic volume and reduced LV ejection fraction in the High group were restored to the levels of the Low group by culturing intact CSCs under High+GSI conditions for 3 passages before transplantation. These findings suggested the reduced therapeutic potential of the High group was mediated by Notch signaling activation during cultivation, which compromised the multipotency of CSCs through EC differentiation.

LV Remodeling and Angiogenesis After CSC Transplantation

Because the therapeutic potential of CSCs is dependent not only on multipotency but also paracrine effects, the latter (LV remodeling and angiogenesis) were further assessed histologically at 3 weeks after transplantation. We expected CSCs cultured under Low and High+GSI conditions to show greater paracrine effects than those under High conditions.

The Low and High+GSI groups had reduced area of scarring and preserved structure of LV compared with the High group, which showed a similar scar size and structure to the PBS-only group, as assessed by Masson's trichrome staining (**Figure 4D**). The percentage of fibrosis in the LV was significantly less in the Low and High+GSI groups compared with the PBS-only and High groups (**Figure 4F**). vWF-positive arterioles and capillaries were more prominent in the infarct-border zone of the Low, High and High+GSI groups compared with the PBS-only group (**Figures 4E,G**). These results indicated that not only direct differentiation potential (multipotency) but also the paracrine effect (antifibrotic effect) of the Low and High+GSI groups might be greater than those of the High group.

Differentiation Potential of CSCs in Vivo

Finally, we examined whether the greater multipotency of the Low and High+GSI groups in vitro reflected greater therapeutic potential in vivo as compared with the High group. The phenotypic fate of the transplanted CSCs, in relation to their plating cell-density and Notch signaling, was assessed in excised rat hearts at 3 weeks after transplantation.

MLC and HNA-double-positive cells were present in the infarct-border zone of the Low and High+GSI groups, but were rarely detected in the High group (**Figure 5A**). Quantitative assessment showed that 60% of the HNA-positive transplanted

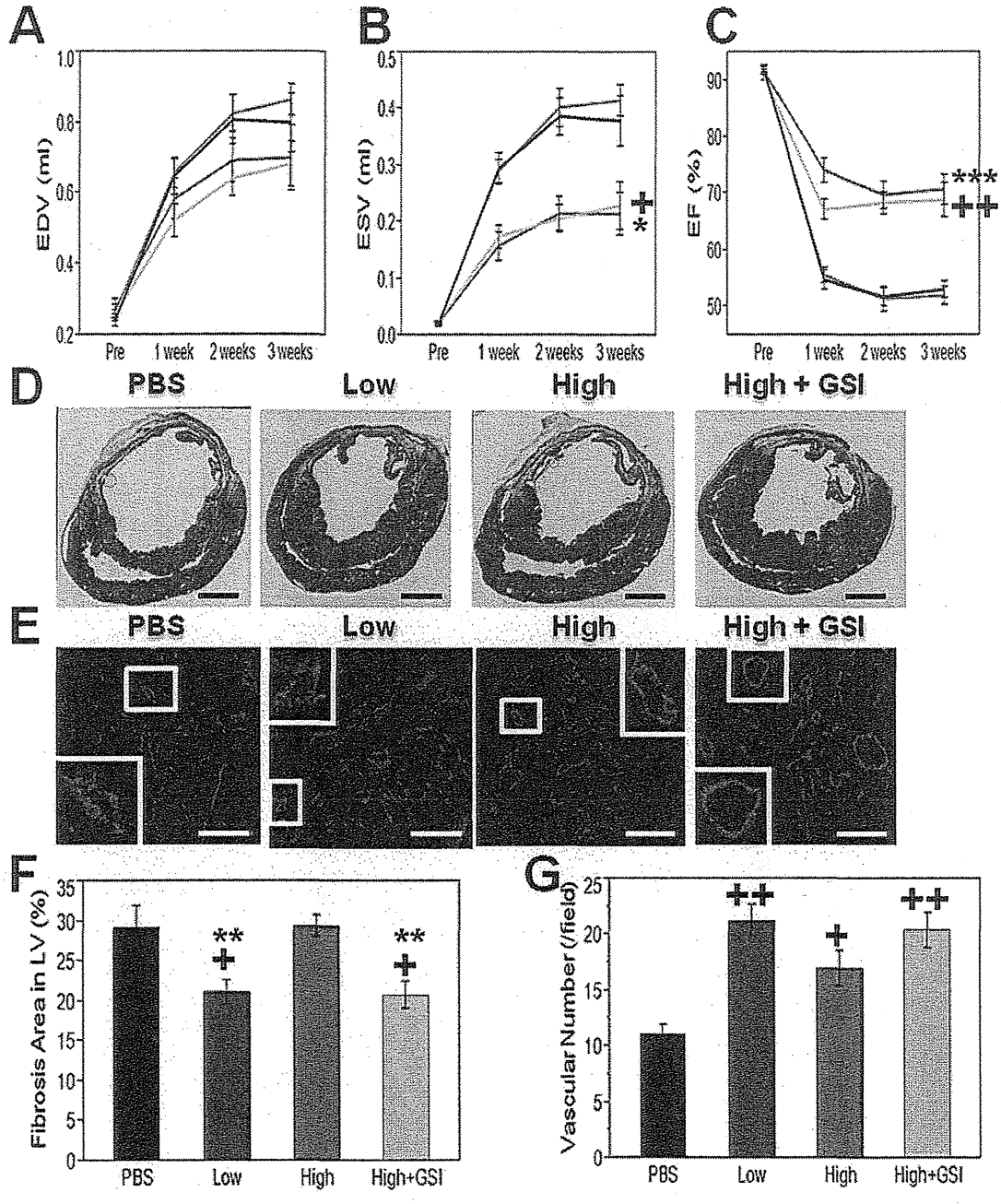

Figure 4. Therapeutic potential of cardiac stem cells in a rat model of acute myocardial infarction. (**A–C**) Echocardiography before (Pre) and after transplantation (1, 2, or 3 weeks). (**A**) End-diastolic volume (EDV, ml), (**B**) end-systolic volume (ESV, ml), (**C**) ejection fraction (EF, %) of rat left ventricle. Black lines indicate PBS treatment, blue lines "Low", red lines "High", and yellow lines "High+GSI" group. The results from 9–11 rats per group were examined. *P<0.05, ***P<0.0001 Low vs. "PBS" and "High" groups. +P<0.05, ++P<0.01 High+GSI vs. "PBS" and "High" groups. (**D–E**) Masson's trichrome staining and immunostaining against vWF. The insets show the enlarged image of the indicated area. Scale bars=2mm in (**D**) and 200μm in (**E**). (**F–G**) Quantitative analysis of D and E. (**F**) The results from 9–11 sections at the mid-ventricle level (transplanted site) from 9–11 rats per group were analyzed. (**G**) The results from 54–66 fields from 9–11 rats per group were analyzed. **P<0.01 vs. "High" group. +P<0.05, ++P<0.01 vs. "PBS" group. PBS, phosphate-buffered saline; vWF, von Willebrand factor.

cells in the Low group and 70% in the High plus GSI group were positive for MLC, compared with the High group in which only 20% of the HNA-positive cells were MLC-positive (**Figure 5B**). In addition, the human-derived cardiomyocytes survived at least for 3 weeks after transplantation and resided mainly in the infarct-border zone. These results indicated that the lower plating density with lower Notch signaling maintained the multipotency of CSCs in vitro and their cardiomyogenic differentiation potential in vivo, which resulted in a greater therapeutic potential in the rat model of AMI.

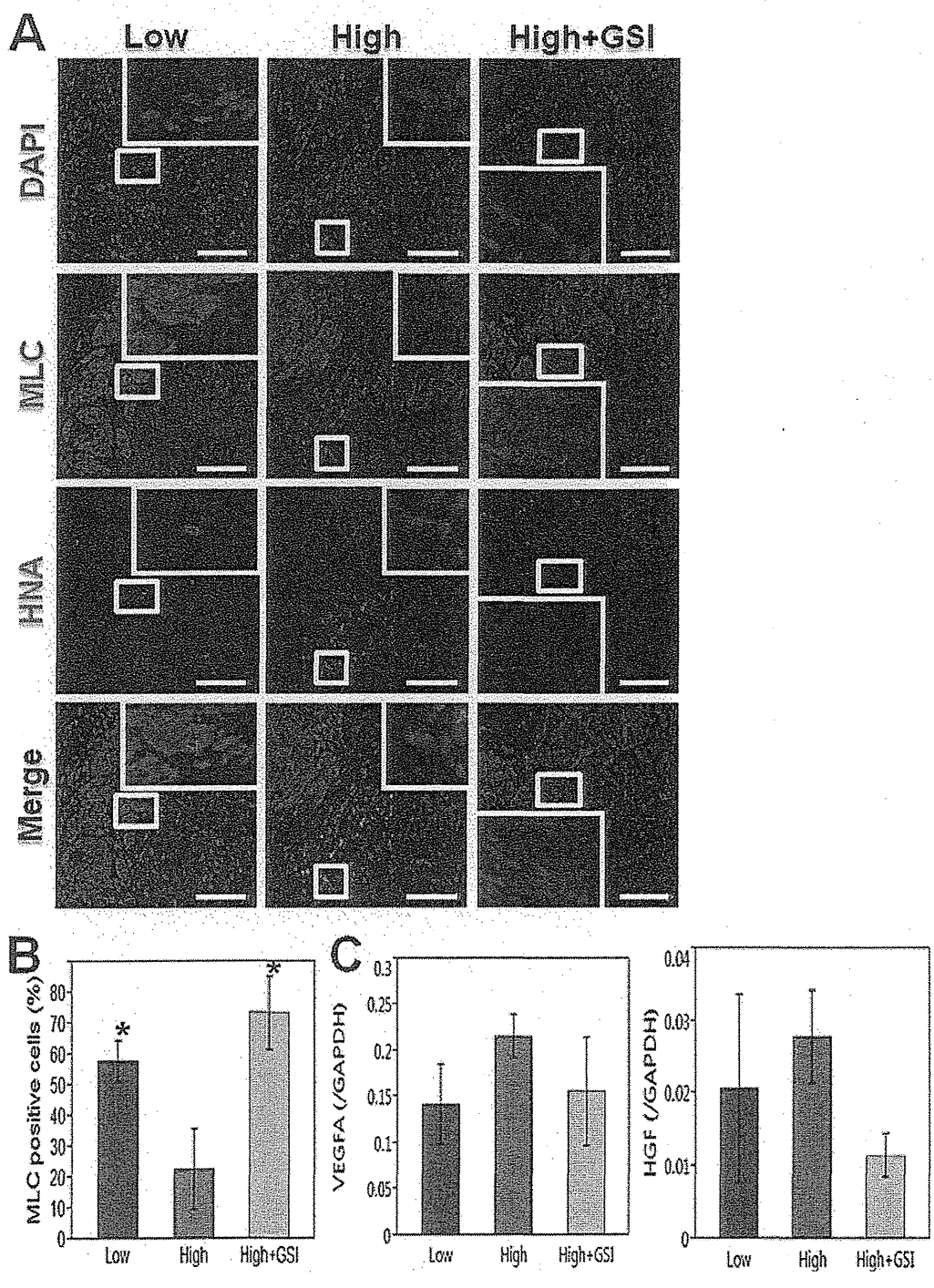

Figure 5. Differentiation potential of cardiac stem cells into cardiomyocytes in vivo. (**A**) Representative images for immunostaining against myosin light chain (MLC, red) and human nuclear antigen (HNA, green). DAPI (blue) was used for nuclear staining. Scale bars=100μm. (**B**) Quantitative analysis of HNA-positive cells that were MLC-positive in vivo. The results from 10–31 fields per group (from 2–4 rats per group) were analyzed. *P<0.05 vs. "High" group. (**C**) qPCR analysis for VEGFA and HGF. Rat hearts were collected at 2 days after transplantation. GAPDH was used as internal control; 3–4 rats per group were used.

Regarding the paracrine effects, we examined by qPCR some paracrine factors (VEGFA and HGF)[4] at 2 days after transplantation. These experiments showed no significant difference in the expression levels of the paracrine factors among the groups (**Figure 5C**).

Discussion

We discovered that Notch signaling was activated in CSCs under high cell-plating conditions and induced EC differentiation. Notch signaling is implicated as a key regulator of arte-

rial EC differentiation from Flk1-positive endothelial precursors.[28] In addition, VEGF is a known key regulator of EC differentiation from embryonic stem cells.[29] In this study, VEGFA and Notch signaling were both activated in the High group (**Figures 2A,D**). Moreover, the use of GSI clearly dissected the difference in downstream angiogenic gene expressions and in angiogenic potential between the low- and high-density cultures (**Figures 2C,E,F**). Thus, the results from this study lead to the conclusion that Notch signaling is involved in the EC differentiation of CSCs.

C-KIT positivity was markedly reduced during cultivation regardless of the plating cell-density in this study, though previous reports suggested that C-KIT positivity was preserved for several passages until transplantation.[3,7] This contrary finding between the present and the previous studies may be explained by different patient population, sampling/isolation protocols, culture protocols including plating cell-density, and/or different C-KIT detection protocols.[3,7] Although a direct relationship between C-KIT positivity and the therapeutic effects of CSCs remains unclear, plating cell-density was related to C-KIT positivity and therapeutic effects in this study, warranting further studies to investigate the significance of C-KIT expression in this treatment. In addition, the absolute number of C-KIT positive cells increased under low-density conditions compared with the high-density conditions (**Figure S1A**). Thus, low-density conditions might propagate CSCs effectively. In addition, we confirmed that CSCs expressed KDR but not Nkx2.5 (**Figure S3C**). Therefore, the characteristics of CSCs might be similar to those of cardiovascular progenitors.[12,30]

The findings of this study suggested that plating cell-density was a determinant of in vitro fundamental cellular function, including multipotency and the in vivo therapeutic effects of CSCs, and that Notch signal is one of the mechanisms responsible for this plating density-dependent function. CSCs that were cultured under High conditions showed a trend in EC differentiation with loss of SC properties such as multipotency. Although this spontaneous differentiation of CSCs was associated with activation of the Notch signaling pathway, inhibition of Notch signaling using GSI did not totally restore cellular function, including C-KIT positivity and PDT (**Figure S1B**).

One may consider several reasons for this as follows. Firstly, the Notch signal pathway was not totally inhibited by GSI treatment, though the concentration of GSI was carefully prepared by referring to a previous report[16] and doing preliminary experiments (**Figures S1C–E**). Secondly, alternative pathways to Notch signaling are present that may affect cellular properties in the maintenance culture of CSCs.[17,25,31] Finally, Notch signaling in the Low group might be slightly activated during the culture process and thus affect the properties of CSCs.

The magnitude of the therapeutic effects of CSCs in the rat AMI model was dependent upon the plating density in association with Notch signaling in this study. Although inhibition of Notch signaling in the High group did not totally restore cellular functions in vitro (**Figures 2D,3E**), functional and pathological recovery from AMI in the High group was totally restored by inhibition of Notch signaling during the course of cell preparation. This contrary finding may be explained by differences in cellular functions between in vitro and after transplantation into a rat AMI model. The cells that were transplanted into the heart were influenced by a variety of factors, such as needle injection-related mechanical damage, ischemia, inflammation or factors released from the native cardiac tissue.[32,33] These complex pathways in this treatment may yield different results for in vitro and in vivo experiments.

Regarding the therapeutic potential of CSCs, not only the cardiomyogenic potential but also differentiation potential into other lineages or just the proliferative activity of the cells might be considered. However, only a few CSC-derived vWF-positive ECs were detected (**Figure S2A**). For the SMCs, a significant difference in the percentage of αSMA-positive cells was observed between not only the Low and High groups but also the Low and High+GSI groups (**Figure S2B**). In addition, the difference in proliferative activity in vitro might not explain the difference in therapeutic potential between the Low and High groups because the High+GSI group did not recover PDT (**Figure S1B**). Therefore, we conclude that the cardiomyogenic differentiation potential might be the main difference between the Low and High groups in terms of therapeutic potential, which was affected by Notch signaling.

In addition, we also examined the paracrine effect of transplanted CSCs and observed no significant difference in the VEGFA or HGF (**Figure 5C**) (and IGF1; **Figure S2C**) expression levels[4] among the groups (Low vs. High vs. High+GSI) at 2 days after transplantation. This was contrary to results shown in **Figures 4D,F**, which indicated that the antifibrotic effect (possibly by paracrine mechanisms) was hampered by culturing CSCs at a higher plating density. Therefore, other unknown factor(s) might be present and the "High" culture condition might hamper the expression of such protein(s) after transplantation.

This study is limited by the use of primary CSCs from mainly 1 individual patient who had idiopathic cardiomyopathy (except qPCR for C-KIT, IL-8, and VEGFA, in which 3 different patients' samples were used; **Figures 2B–D**), though a consistent fundamental difference in the cellular behavior of primary CSCs cultured with different plating densities was confirmed (PDTs with 4 different patient samples and C-KIT positivity with another patient sample; **Figures S3A,B**).

Regarding CSC preparation in the clinical scenario, the use of Notch signaling inhibitor in the culture process may be useful in enhancing the therapeutic potential of CSCs.[34] In addition, regarding the duration of the existence and localization of the transplanted cells, human-derived cardiomyocytes survived at least for 3 weeks after transplantation and resided mainly in the infarct-border zone. In this study, CSCs of human origin were transplanted into athymic nude rats. This xenotransplantation model has been used in a number of studies, which have rarely reported significant immunological reactions.[22,35] In fact, the transplanted cells in this study were not histologically involved in inflammatory reactions such as accumulation of inflammatory cells (data not shown). Thus, immune rejection in this model is minimal and does not affect the results. In addition, CSCs will be transplanted in an autologous manner in the clinical situation.[6] Therefore, the immunological reactions of this treatment may be negligible.

In conclusion, cellular properties and therapeutic potential of CSCs are affected by cell-plating density through activation of Notch signaling. Therapeutic effects of CSC-transplantation therapy for heart disease may be enhanced by reducing Notch signaling in CSCs.

Acknowledgments

This study was financially supported by a Health Labor Sciences Research Grant from the Japanese Ministry of Health, Labor and Welfare. T.M. was supported by a Grant-in-Aid from the Japan Society for the Promotion of Science Fellows. We thank Professor Piero Anversa (Brigham and Women's Hospital, Boston, USA) and his laboratory members for technical advice. We also thank Ms Masako Yokoyama for technical instruction, Ms Atsuko Shimai and Ms Yuka Takaoka (all from Osaka University), and Ms

Noriko Kakuta (Institute of Biomedical Research and Innovation) for assistance with the manuscript.

References

1. Roger VL, Go AS, Lloyd-Jones DM, Adams RJ, Berry JD, Brown TM, et al. Heart disease and stroke statistics: 2011 update. A report from the American Heart Association. *Circulation* 2011; **123:** e18–e209, doi:10.1161/CIR.0b013e3182009701.
2. Yamauchi T, Miyata H, Sakaguchi T, Miyagawa S, Yoshikawa Y, Takeda K, et al. Coronary artery bypass grafting in hemodialysis-dependent patients: Analysis of Japan Adult Cardiovascular Surgery Database. *Circ J* 2012; **76:** 1115–1120.
3. Bearzi C, Rota M, Hosoda T, Tillmanns J, Nascimbene A, De Angelis A, et al. Human cardiac stem cells. *Proc Natl Acad Sci USA* 2007; **104:** 14068–14073.
4. Chimenti I, Smith RR, Li TS, Gerstenblith G, Messina E, Giacomello A, et al. Relative roles of direct regeneration versus paracrine effects of human cardiosphere-derived cells transplanted into infarcted mice. *Circ Res* 2010; **106:** 971–980.
5. Choi SH, Jung SY, Kwon SM, Baek SH. Perspectives on stem cell therapy for cardiac regeneration: Advances and challenges. *Circ J* 2012; **76:** 1307–1312.
6. Bolli R, Chugh AR, D'Amario D, Loughran JH, Stoddard MF, Ikram S, et al. Cardiac stem cells in patients with ischaemic cardiomyopathy (SCIPIO): Initial results of a randomised phase 1 trial. *Lancet* 2011; **378:** 1847–1857.
7. D'Amario D, Fiorini C, Campbell PM, Goichberg P, Sanada F, Zheng H, et al. Functionally competent cardiac stem cells can be isolated from endomyocardial biopsies of patients with advanced cardiomyopathies. *Circ Res* 2011; **108:** 857–861.
8. Bartosh TJ, Wang Z, Rosales AA, Dimitrijevich SD, Roque RS. 3D-model of adult cardiac stem cells promotes cardiac differentiation and resistance to oxidative stress. *J Cell Biochem* 2008; **105:** 612–623.
9. Tang YL, Zhu W, Cheng M, Chen L, Zhang J, Sun T, et al. Hypoxic preconditioning enhances the benefit of cardiac progenitor cell therapy for treatment of myocardial infarction by inducing CXCR4 expression. *Circ Res* 2009; **104:** 1209–1216.
10. Messina E, De Angelis L, Frati G, Morrone S, Chimenti S, Fiordaliso F, et al. Isolation and expansion of adult cardiac stem cells from human and murine heart. *Circ Res* 2004; **95:** 911–921.
11. Tomita Y, Matsumura K, Wakamatsu Y, Matsuzaki Y, Shibuya I, Kawaguchi H, et al. Cardiac neural crest cells contribute to the dormant multipotent stem cell in the mammalian heart. *J Cell Biol* 2005; **170:** 1135–1146.
12. Yang L, Soonpaa MH, Adler ED, Roepke TK, Kattman SJ, Kennedy M, et al. Human cardiovascular progenitor cells develop from a KDR+ embryonic-stem-cell-derived population. *Nature* 2008; **453:** 524–528.
13. Bu L, Jiang X, Martin-Puig S, Caron L, Zhu S, Shao Y, et al. Human ISL1 heart progenitors generate diverse multipotent cardiovascular cell lineages. *Nature* 2009; **460:** 113–117.
14. Sekiya I, Larson BL, Smith JR, Pochampally R, Cui JG, Prockop DJ. Expansion of human adult stem cells from bone marrow stroma: Conditions that maximize the yields of early progenitors and evaluate their quality. *Stem Cells* 2002; **20:** 530–541.
15. Yanagisawa M, Mukai A, Shiomi K, Song SY, Hashimoto N. Community effect triggers terminal differentiation of myogenic cells derived from muscle satellite cells by quenching Smad signaling. *Exp Cell Res* 2011; **317:** 221–233.
16. Boni A, Urbanek K, Nascimbene A, Hosoda T, Zheng H, Delucchi F, et al. Notch1 regulates the fate of cardiac progenitor cells. *Proc Natl Acad Sci USA* 2008; **105:** 15529–15534.
17. Chen VC, Stull R, Joo D, Cheng X, Keller G. Notch signaling respecifies the hemangioblast to a cardiac fate. *Nat Biotechnol* 2008; **26:** 1169–1178.
18. Kwon C, Qian L, Cheng P, Nigam V, Arnold J, Srivastava D. A regulatory pathway involving Notch1/beta-catenin/Isl1 determines cardiac progenitor cell fate. *Nat Cell Biol* 2009; **11:** 951–957.
19. Obi S, Masuda H, Shizuno T, Sato A, Yamamoto K, Ando J, et al. Fluid shear stress induces differentiation of circulating phenotype endothelial progenitor cells. *Am J Physiol Cell Physiol* 2012; **303:** C595–C606.
20. Gomes SA, Rangel EB, Premer C, Dulce RA, Cao Y, Florea V, et al. S-nitrosoglutathione reductase (GSNOR) enhances vasculogenesis by mesenchymal stem cells. *Proc Natl Acad Sci USA* 2013; **110:** 2834–2839.
21. Imanishi Y, Saito A, Komoda H, Kitagawa-Sakakida S, Miyagawa S, Kondoh H, et al. Allogenic mesenchymal stem cell transplantation has a therapeutic effect in acute myocardial infarction in rats. *J Mol Cell Cardiol* 2008; **44:** 662–671.
22. Iwasaki H, Kawamoto A, Ishikawa M, Oyamada A, Nakamori S, Nishimura H, et al. Dose-dependent contribution of CD34-positive cell transplantation to concurrent vasculogenesis and cardiomyogenesis for functional regenerative recovery after myocardial infarction. *Circulation* 2006; **113:** 1311–1325.
23. Bray SJ. Notch signalling: A simple pathway becomes complex. *Nat Rev Mol Cell Biol* 2006; **7:** 678–689.
24. Urbanek K, Cabral-da-Silva MC, Ide-Iwata N, Maestroni S, Delucchi F, Zheng H, et al. Inhibition of notch1-dependent cardiomyogenesis leads to a dilated myopathy in the neonatal heart. *Circ Res* 2010; **107:** 429–441.
25. Zakharova L, Nural-Guvener H, Gaballa MA. Cardiac explant-derived cells are regulated by Notch-modulated mesenchymal transition. *PLoS One* 2012; **7:** e37800, doi:10.1371/journal.pone.0037800.
26. Beltrami AP, Barlucchi L, Torella D, Baker M, Limana F, Chimenti S, et al. Adult cardiac stem cells are multipotent and support myocardial regeneration. *Cell* 2003; **114:** 763–776.
27. Fischer KM, Cottage CT, Wu W, Din S, Gude NA, Avitabile D, et al. Enhancement of myocardial regeneration through genetic engineering of cardiac progenitor cells expressing Pim-1 kinase. *Circulation* 2009; **120:** 2077–2087.
28. Lanner F, Sohl M, Farnebo F. Functional arterial and venous fate is determined by graded VEGF signaling and notch status during embryonic stem cell differentiation. *Arterioscler Thromb Vasc Biol* 2007; **27:** 487–493.
29. Tan KS, Tamura K, Lai MI, Veerakumarasivam A, Nakanishi Y, Ogawa M, et al. Molecular pathways governing development of vascular endothelial cells from ES/iPS Cells. *Stem Cell Rev* 2013 June 14, doi:10.1007/s12015-013-9450-7 [Epub ahead of print].
30. Bearzi C, Leri A, Lo Monaco F, Rota M, Gonzalez A, Hosoda T, et al. Identification of a coronary vascular progenitor cell in the human heart. *Proc Natl Acad Sci USA* 2009; **106:** 15885–15890.
31. Shahi P, Seethammagari MR, Valdez JM, Xin L, Spencer DM. Wnt and Notch pathways have interrelated opposing roles on prostate progenitor cell proliferation and differentiation. *Stem Cells* 2011; **29:** 678–688.
32. Segers VF, Lee RT. Stem-cell therapy for cardiac disease. *Nature* 2008; **451:** 937–942.
33. Dimmeler S, Burchfield J, Zeiher AM. Cell-based therapy of myocardial infarction. *Arterioscler Thromb Vasc Biol* 2008; **28:** 208–216.
34. Coric V, van Dyck CH, Salloway S, Andreasen N, Brody M, Richter RW, et al. Safety and tolerability of the gamma-secretase inhibitor avagacestat in a Phase 2 study of mild to moderate alzheimer disease. *Arch Neurol* 2012; **69:** 1430–1440.
35. Alshammary S, Fukushima S, Miyagawa S, Matsuda T, Nishi H, Saito A, et al. Impact of cardiac stem cell sheet transplantation on myocardial infarction. *Surg Today* 2013 March 5, doi:10.1007/s00595-013-0528-2 [Epub ahead of print].

Supplementary Files

Supplementary File 1

Figure S1. C-KIT positive cell number, population doubling time (PDT), and qPCR analysis for cardiac stem cells under different plating densities with and without gamma secretase inhibitor (GSI).

Figure S2. Percentages of transplanted cell-derived differentiated cells in vivo and expression levels of human-specific IGF1 after transplantation.

Figure S3. Population dougling time (PDT) from 4 different patient samples, C-KIT positivity of another patient sample with different plating densities, and RT-PCR analysis for CSCs.

Please find supplementary file(s);
http://dx.doi.org/10.1253/circj.CJ-13-0534

Circulation Journal
Official Journal of the Japanese Circulation Society
http://www.j-circ.or.jp

ORIGINAL ARTICLE
Regenerative Medicine

Myocardial Layer-Specific Effect of Myoblast Cell-Sheet Implantation Evaluated by Tissue Strain Imaging

Yasuhiro Shudo, MD; Shigeru Miyagawa, MD, PhD; Satoshi Nakatani, MD, PhD; Satsuki Fukushima, MD, PhD; Taichi Sakaguchi, MD, PhD; Atsuhiro Saito, PhD; Toshihiko Asanuma, MD, PhD; Naomasa Kawaguchi, PhD; Nariaki Matsuura, MD, PhD; Tatsuya Shimizu, MD, PhD; Teruo Okano, PhD; Yoshiki Sawa, MD, PhD

Background: The implantation of skeletal myoblast (SMB) cell-sheets over the damaged area of a myocardial infarction (MI) has been shown to improve global left ventricular (LV) function through a paracrine effect. However, the regeneration process has not been fully evaluated. We hypothesized that the use of tissue Doppler strain M-mode imaging to assess myocardial layer-specific strain might enable detailed visual evaluation of the regenerative ability of SMBs.

Methods and Results: SMBs were cultured on temperature-responsive culture dishes to generate cell-sheets. At 4 weeks after inducing anterior MI, the animals were divided into 2 groups: SMB cell-sheet implantation and sham operation (n=6 in each). A total of 30 cell-sheets (1.5×10^7 cells/sheet) were placed on the epicardium, covering the infarct and border regions. Subendocardial and subepicardial strain values were measured in the infarct, border, and remote regions by tissue Doppler strain analysis. SMB cell-sheet implantation produced the following major effects: progression of LV remodeling was prevented and global LV ejection fraction increased; the subendocardial strain was significantly greater than the subepicardial strain in the treated border region; vascular density in the subendocardium was significantly higher than in the subepicardium in the treated region; the expression of vascular endothelial growth factor was significantly increased.

Conclusions: Tissue Doppler strain analysis allows precise evaluation of the effect of cell-sheet implantation on layer-specific myocardial function. (*Circ J* 2013; **77:** 1063–1072)

Key Words: Cytokines; Heart failure; Strain; Tissue Doppler

Heart failure still occurs frequently and is life-threatening, despite recent medical and surgical advances. Myocardial regenerative therapy is attracting growing interest as a means of improving left ventricular (LV) function in advanced heart failure.[1–3] However, recent clinical trials reported slightly disappointing results for cell transplantation by needle injection.[2–4] The major drawbacks of cell transplantation using that technique are poor retention and survival of the injected cells, local myocardial damage and potential lethal arrhythmias. The cell-sheet technique was developed to deliver cells efficiently without damaging the myocardium and, consequently, more effectively improve cardiac function than the needle injection method.[5–9] This therapeutic modality is already being used in the clinical setting.[10] It has been suggested that implantation of a skeletal myoblast (SMB) cell-sheet reverses LV remodeling via paracrine effects in which angiogenic factors constitutively released from the implanted cell-sheets induce neo-angiogenesis, increased vascular density and blood flow, thereby reversing hybernating myocardium.[5–10] However, detailed evaluation of functional improvement (eg, region-specific functional recovery associated with secreted cytokines) has not been performed. Moreover, the existing evidence base remains inconsistent, and the underlying mechanism and optimal protocols are still being debated.[11]

Tissue strain M-mode imaging based on the tissue Doppler technique (TDI-Q, Toshiba) was developed to accurately mea-

Received May 24, 2012; revised manuscript received October 15, 2012; accepted November 20, 2012; released online December 29, 2012 Time for primary review: 24 days

Department of Cardiovascular Surgery (Y. Shudo, S.M., S.F., T. Sakaguchi, A.S., Y. Sawa), Department of Health Sciences, Division of Functional Diagnostics (S.N., T.A.), Department of Pathology (N.K., N.M.), Osaka University Graduate School of Medicine, Suita; and Advanced Biomedical Engineer and Science, Tokyo Women's Medical University, Tokyo (T. Shimizu, T.O.), Japan

Presented at the American College of Cardiology's 60th Annual Scientific Session, ACCF/Herman K. Gold Young Investigator's Award in Molecular and Cellular Cardiology, New Orleans, LA, April 2–5, 2011.

Mailing address: Yoshiki Sawa, MD, PhD, Department of Cardiovascular Surgery, Osaka University Graduate School of Medicine, 2-15 Yamada-oka, Suita 565-0871, Japan. E-mail: sawa-p@surg1.med.osaka-u.ac.jp

ISSN-1346-9843 doi:10.1253/circj.CJ-12-0615

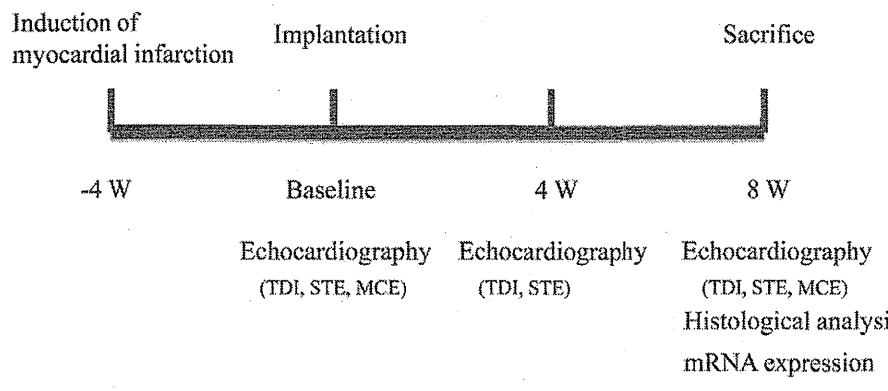

Figure 1. Study protocol for the assessment of cardiac function and histological analysis. TDI, tissue Doppler imaging; STE, speckle tracking echocardiography; MCE, myocardial contrast echocardiography.

sure myocardial layer-specific strain values, based on the transmural myocardial strain profile (TMSP).[12–14] Within the myocardium, the specific characteristics of each myocardial layer confer a different ability to improve regional myocardial performance.[15] We hypothesized that the myocardial layer-specific strain values might enable an assessment of regional functional improvement, based on the paracrine effects of cytokines following cell-sheet implantation. To investigate our hypothesis, we assessed the TMSP in a porcine model of myocardial infarction (MI).

Methods

Ethics

All studies were performed with the approval of the Ethics Committee of Osaka University. Humane animal care was used in compliance with the "Principles of Laboratory Animal Care" formulated by the National Society for Medical Research and the "Guide for the Care and Use of Laboratory Animals" prepared by the Institute of Animal Resources and published by the National Institutes of Health (Publication No 85-23, revised 1996). All authors had full access to the data and take full responsibility for its integrity. All authors have read and agreed to the manuscript as written. All procedures and evaluations, including the assessment of cardiac parameters, were carried out in a blinded manner.

Animal Models and Study Protocol (Figure 1)

We used 20 female mini-pigs (8–10 months old, 20–25 kg; Japan Farm Co Ltd, Kagoshima, Japan). They were anesthetized with intravenous ketamine (6 mg/kg) and sodium pentobarbital (10 mg/kg) for endotracheal intubation and then maintained with inhaled sevoflurane (1–2%). The pericardial space was exposed by left thoracotomy through the 4th intercostal space. The distal portion of the left anterior descending coronary artery (LAD) was directly ligated, followed by placement of an ameroid constrictor around the LAD just distal of the branching of the left circumflex coronary artery (LCX) to prevent sudden cardiac death from lethal ventricular arrhythmia and intolerance of ischemia.[5,16] This technique produces an MI model that has clinical relevance and can be used for appropriate preclinical studies with minimal procedure-related mortality (6 (30%) of the 20 mini-pigs died within 48 h of surgery primarily from acute cardiac failure).

Computer-generated random allocation generated 2 randomized study groups at 1 week after the induction of MI, and autologous cells were then isolated and grown in culture for 3 weeks for implantation. At 4 weeks after MI induction, the mini-pigs were again placed under general anesthesia for echocardiography followed by either cell-sheet implantation or sham operation. Two mini-pigs in which the LV ejection fraction (LVEF) was >40%, measured by transthoracic echocardiography using the Simpson's method before the treatment, were excluded from the study. At 4 and 8 weeks after either cell-sheet implantation or sham operation, the mini-pigs were again placed under general anesthesia for echocardiography examination. The mini-pigs were killed humanely following the 8-week echocardiography study for histological and biochemical analysis of the heart tissue.

Preparing and Grafting Skeletal Myoblast Cell Sheets

Autologous skeletal muscle weighing approximately 10–15 g was removed from the quadriceps femoris muscle, and purified autologous SMB cells were cultured for 3 weeks in preparation for implantation as described previously.[5] The cells were incubated in 60-mm temperature-responsive culture dishes (UpCell®; Cellseed, Tokyo, Japan) at 37°C for 24 h, with the cell numbers adjusted to 1.5×10^7 cells/dish. The dishes were then transferred to another incubator set at 20°C for 1 h to release the cultured cells as intact cell-sheets. SMB spontaneously detached to generate free-floating monolayer cell-sheets.

At 4 weeks after MI induction, the mini-pigs were randomly divided into the 2 treatment groups (n=6 in each): SMB cell-sheet implantation (Sheet group) or sham operation (Sham group). In the Sheet group, 30 cell-sheets (1.5×10^7 cells/sheet) with the total cell number being 4.5×10^8 were implanted on the epicardium of the ischemic area (LAD region) via median sternotomy approach under general anesthesia. Cell sheets were attached and fixed to the epicardial surface by stitching around the edge of the sheet.

Conventional Echocardiography

Global cardiac function was assessed using a commercially available echocardiograph machine with a 4.0-MHz transducer (Aplio; Toshiba, Otawara, Japan) before, and 4 and 8 weeks after cell-sheet implantation. Echocardiographic measurements included LV end-diastolic and end-systolic volumes (LVEDV

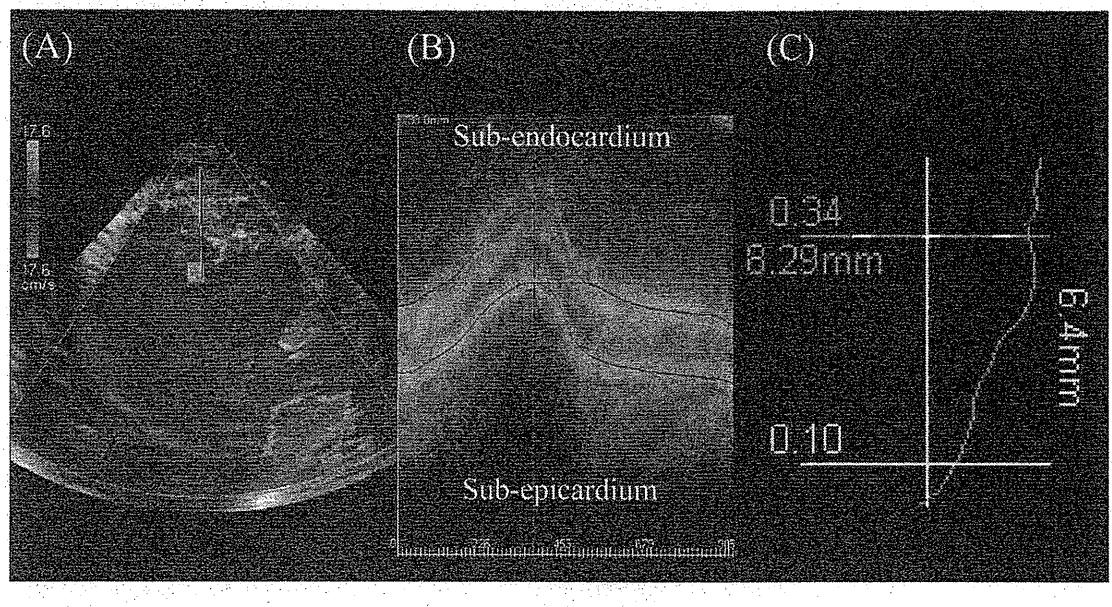

Figure 2. Measurement of transmural myocardial strain profile by tissue strain M-mode imaging and the indicated analysis software. (**A**) Recordings stored in the form of digital loops of 2 cardiac cycles for subsequent offline analysis. (**B**) LV endocardium and epicardium traced from an end-systolic frame. (**C**) Endocardial and epicardial borders automatically tracked through 1 cardiac cycle using analysis software (TDI-Q; Toshiba, Tokyo, Japan).

and LVESV, respectively), and LVEF, calculated as:

$$EF\,(\%) = 100 \times (LVEDV - LVESV)/(LVEDV).$$

Myocardial Layer-Specific Strain Using Tissue Doppler Strain M-Mode Imaging

Tissue strain M-mode imaging (frame rate, 82–118 frames/s) based on the tissue Doppler technique and the corresponding analysis software (TDI-Q, Toshiba, Otawara, Japan) were used to assess myocardial layer-specific strain. Parasternal short-axis images were recorded at the level of base, mid-ventricle, and apex by tissue Doppler imaging (**Figure 2A**). To obtain a strain image, TDI-Q first calculates the myocardial displacement of all pixels of tissue by integrating myocardial velocity over a certain period. Next, strain is obtained by evaluating the change in the distance between pairs of points defined on all pixels of the image by utilizing the displacement values. The initial time frame is set at end-diastole to evaluate myocardial deformation occurring in systole. To measure local strain accurately, it is essential to accurately obtain local velocity. Therefore, the present imaging system used tissue Doppler tracking and angle-correction techniques. Tissue Doppler tracking is an automatic motion tracking technique based on tissue Doppler information. By integrating the velocity of an index point on the ventricular wall, identified from tissue Doppler imaging, we could obtain myocardial displacement and predict where the index point would move next. By repeating this procedure, the system can automatically track the motion of the index point (**Figure 2B**). With this technique, the influence of myocardial translation can be ignored. The angle-correction technique enables Doppler incident angle dependency to be partially overcome. To correct the Doppler incident angle, a contraction center is set at the center of the LV cavity at end-systole in the short-axis view. The software automatically calculates the tissue velocity toward the contraction center (V motion) by dividing the velocity toward a transducer (V beam) by the cosine of the angle (θ) between the Doppler beam and the direction to the contraction center as follows:

$$V\ \text{motion} = V\ \text{beam}/\cos\theta$$

Using these 2 techniques, the software TDI-Q automatically cancelled the effect of myocardial translation and angle dependency, accurately assessing myocardial velocity, displacement, and strain. In previously described experiments, the displacement data obtained by this method correlated with true displacement.[17] Myocardial radial strain distribution over the myocardium is obtained as M-mode color-coded images and the profile of distribution (TMSP) at end-systole is shown as in **Figure 2C**. We divided the myocardium into subendocardial and subepicardial half-layers by the mid-point of the myocardium at end-systole. Mean strain values in the subendocardial half-layer and in the subepicardial half-layer were calculated by averaging the strain values over each layer in the infarcted (center of segment 13), border (edge of segment 7),[18] and remote regions (center of segment 10). In this study, the "infarcted" region was assigned predominantly to territories of the LAD, and the "remote" region was assigned to the LCX or right coronary artery.

Histological and Immunohistochemical Analyses

At 8 weeks after the treatment, the hearts were dissected and embedded in optimum cutting temperature compound, snap-frozen in liquid nitrogen, and cut into sections. The 5-μm-thick, paraffin-embedded sections fixed in 4% paraformaldehyde were stained with hematoxylin-eosin (HE) or Masson's trichrome. Using Image J software, the infarcted area was expressed as a percentage calculated as the positively stained LV area/total LV area in sections stained with Masson's trichrome. The 5-μm thick cryosections fixed in 4% paraformaldehyde were immunofluorolabeled with anti-von Willebrand factor

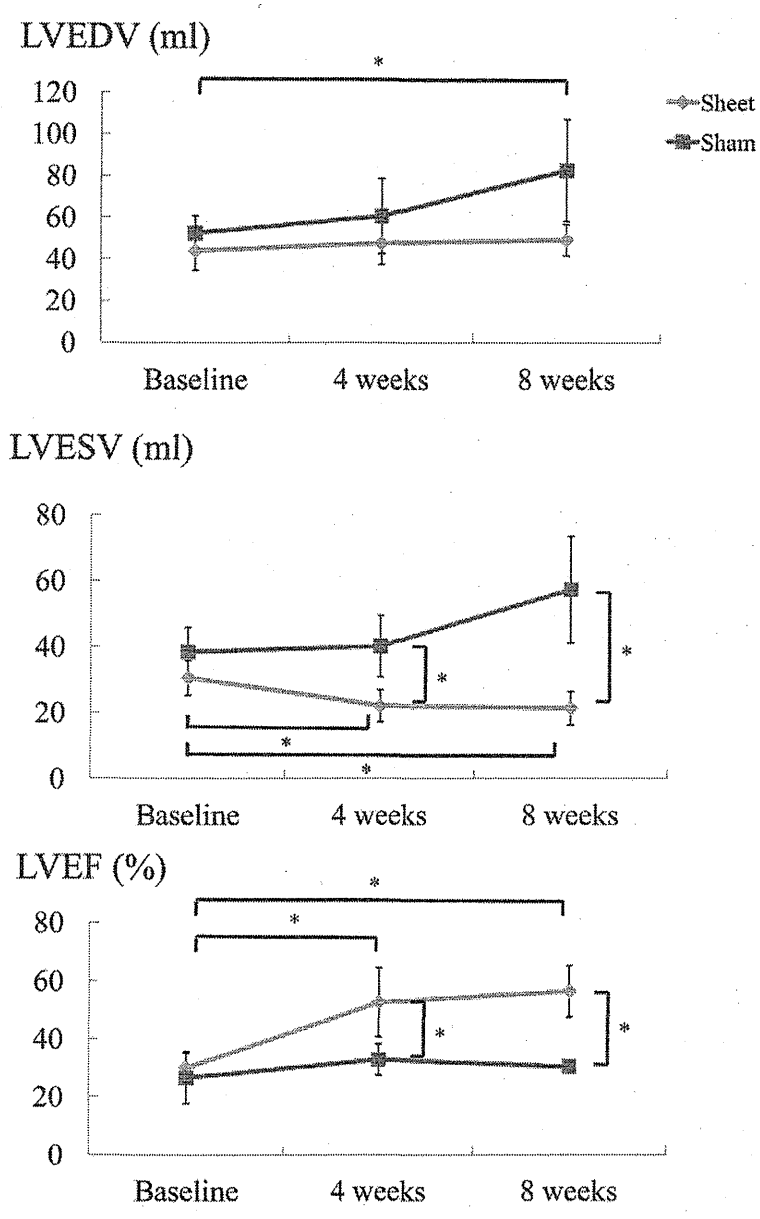

Figure 3. Echocardiographic analysis. LVEDV increased significantly at 8 weeks in the Sham group compared with baseline, and remained unchanged in the Sheet group. LVESV significantly decreased in the Sheet group at 4 and 8 weeks after implantation, showing a significantly lower value than that in the Sham group. LVEF significantly increased in the Sheet group at 4 and 8 weeks after implantation, showing a significantly higher value than that in the Sham group. n=6 in each group; *P<0.05. LVEDV, left ventricular end-diastolic volume; LVESV, left ventricular end-systolic volume; LVEF, left ventricular ejection fraction.

(vWF) antibody (1:250 dilution, Dako, Glostrup, Denmark). The numbers of capillary vessels that were positively stained and 5–10 μm in diameter in the subendocardium and subepicardium of the infarcted, border, and remote regions, in 10 individual, randomly selected fields per heart were counted under high-power magnification (×200) of a BioZero laser scanning microscope (Keyence, Osaka, Japan), then averaged to express vascular density (per mm^2).

Analysis of mRNA Expression

Total RNA was extracted from the border region of cardiac muscle tissue and reverse transcribed into cDNA using TaqMan Reverse Transcription Reagents (Applied Biosystems, Foster City, CA, USA). Real-time polymerase chain reaction (PCR) was performed for vascular endothelial growth factor (VEGF), basic fibroblast growth factor (bFGF), brain natriuretic peptide (BNP), intercellular adhesion molecule-1, tumor necrosis factor-α (TNF-α), interleukin-6 (IL-6), signal transducer and activator of transcription 3, and insulin-like growth factor-1 (IGF-1) using an ABI PRISM 7700 machine.[19] The average copy number of gene transcripts for each sample was normalized to that for GAPDH.

Statistical Analysis

SPSS software (version 11.0, Chicago, IL, USA) was used for statistical analyses. Continuous values are expressed as the mean (standard deviation). The significance of differences was determined using a 2-tailed multiple t-test with Bonferroni correction following repeated measures analysis of variance for individual differences. P<0.05 was considered statistically significant.

Results

Gradual Recovery of Global Systolic LV Function

Serial changes in global systolic and diastolic LV function after cell-sheet implantation were assessed by conventional echo-

Table. Hemodynamics and Strain Measurements

	SMB cell-sheet group (n=6)‡			Sham operation group (n=6)		
	Baseline	4 weeks	8 weeks	Baseline	4 weeks	8 weeks
Heart rate (beats/min)	64±12	66±10	62±13	62±14	62±9	66±14
Blood pressure						
Systolic (mmHg)	98±22	108±25	106±17	102±31	110±28	104±24
Diastolic (mmHg)	70±13	68±9	70±10	68±11	64±10	66±13
Conventional echocardiographic parameters						
End-diastolic volume (ml)	44.1±9.4	47.7±10.2	49.3±7.6	52.5±8.3	60.7±18.0	82.7±24.5*
End-systolic volume (ml)	30.6±5.3	22.1±4.9†,*	21.4±5.1†,*	38.5±7.4	40.2±9.3	57.4±16.2
Ejection fraction (%)	30.1±5.1	52.6±11.9†,*	56.4±8.8†,*	26.6±8.9	32.9±5.4	30.4±1.1
Transmural strain profile using tissue strain imaging						
Border region						
Subendocardial strain (%)	5.73±4.48	27.3±7.64†,*	39.5±8.32†,*	−0.96±1.96	−0.83±2.23	0.71±5.02
Subepicardial strain (%)	8.29±5.56	9.23±7.90	18.5±11.9	8.96±2.05	7.14±2.41	5.37±3.46
Infarct region						
Subendocardial strain (%)	2.77±1.97	6.64±7.90	4.93±4.63	−0.22±3.77	0.77±1.13	−0.21±2.18
Subepicardial strain (%)	−1.40±1.89	2.13±4.37	2.60±2.83	0.02±2.49	0.24±1.15	−0.10±1.07
Remote region						
Subendocardial strain (%)	67.6±17.6	69.2±21.6	75.1±14.3	59.0±4.36	51.8±7.46	46.8±8.29
Subepicardial strain (%)	35.5±12.3	43.3±17.9	53.8±6.91	38.3±8.12	39.9±8.28	35.9±5.47

†P<0.05 vs. Sham group, *P<0.05 vs. Baseline. ‡A total of 30 cell-sheets (1.5×10^7 cells/sheet) were placed on the epicardium, covering the infarct and border regions. SMB, skeletal myoblast.

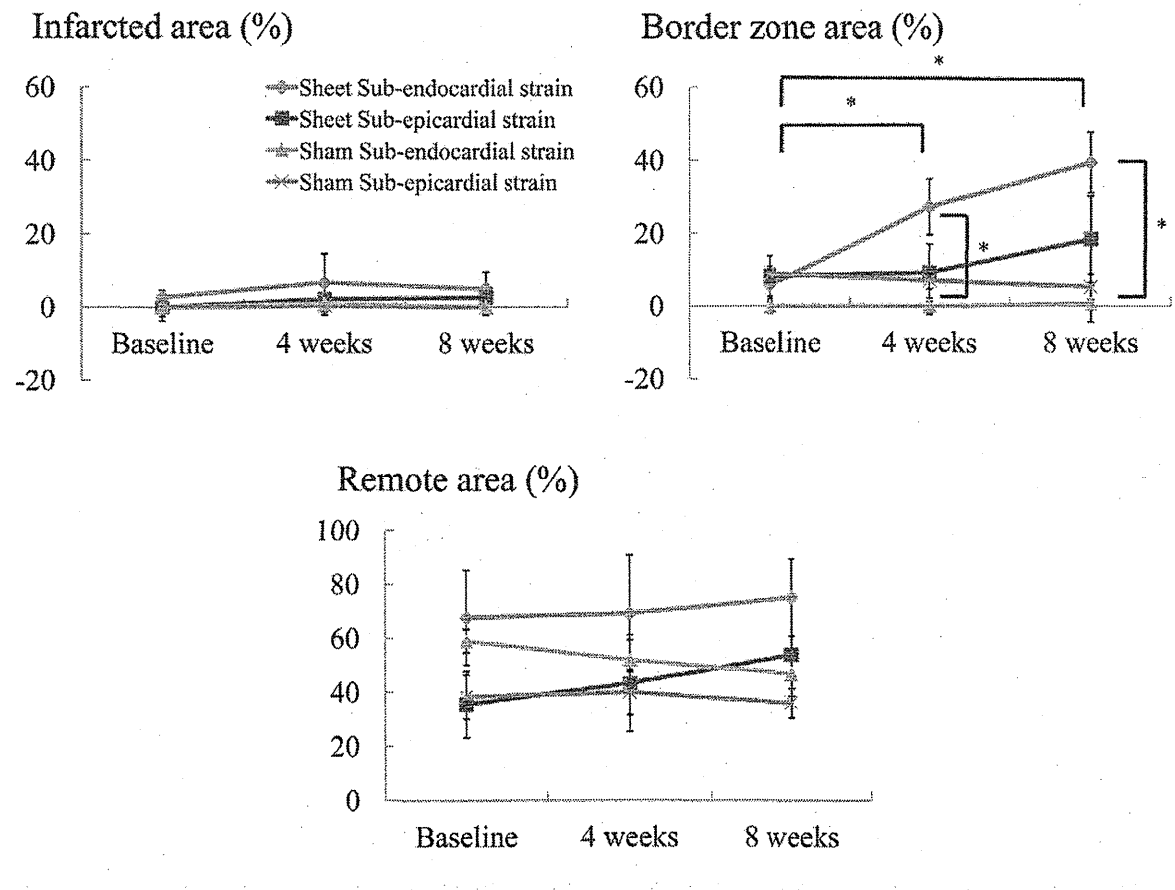

Figure 4. Myocardial layer strain value. In the treated border region, subendocardial strain significantly increased at 4 and 8 weeks after cell-sheet implantation, showing a significant increase in comparison with subepicardial strain. In the infarcted region, both subendocardial and subepicardial strain values were greater in the Sheet group than in the Sham group. In the remote region, no significant changes were observed. n=6 in each group; *P<0.05.

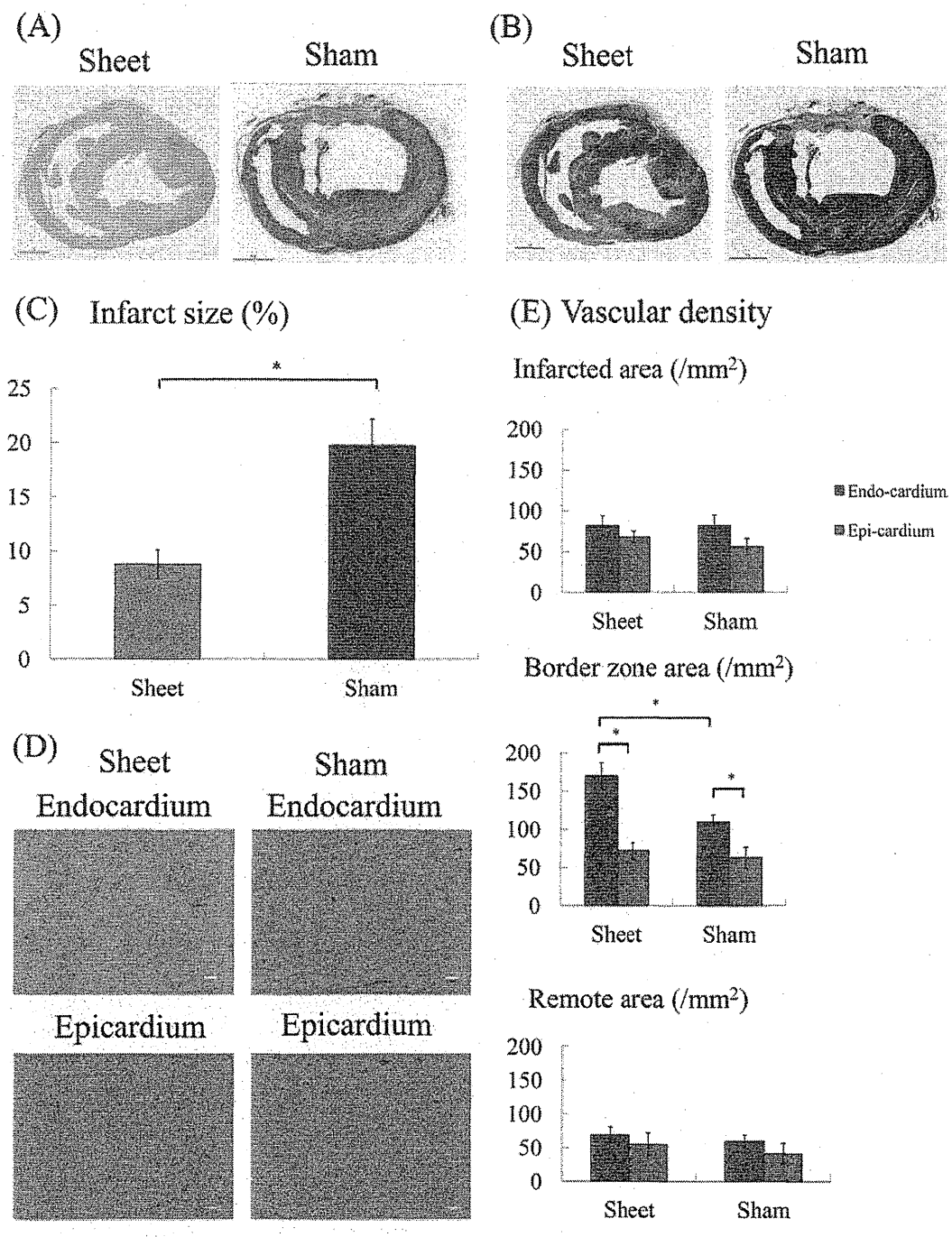

Figure 5. Histological findings. (**A**) Macroscopic (×40) view of the heart (HE). (**B**) Macroscopic (×40) views of the heart (Masson's trichrome). (**C**) The size of the infarcted area of the heart was significantly reduced in the Sheet group as compared with the Sham group. (**D**) Microscopic (×200) views of sections of the subendocardium and subepicardium in the treated border zone area stained with anti-von Willebrand factor (vWF) antibody (factor VIII) (bar=20 μm). (**E**) A greater number of vWF-positive blood vessels in the subendocardium compared with the subepicardium of the border zone area in the Sheet group. No significant changes are seen in the infarcted and remote areas. *P<0.05.

cardiography. Following sham operation, LVEDV and LVESV tended to increase till 8 weeks, while LVEF did not change significantly. In contrast, following SMB cell-sheet implantation, LVEDV did not change significantly, but LVESV significantly decreased and LVEF increased significantly at 4 and 8 weeks after SMB cell-sheet implantation compared with before the implantation. At 4 weeks after the treatment, LVESV was significantly smaller and LVEF was significantly greater in the Sheet group than in the Sham group, but there was no significant difference in LVEDV between them. At 8 weeks

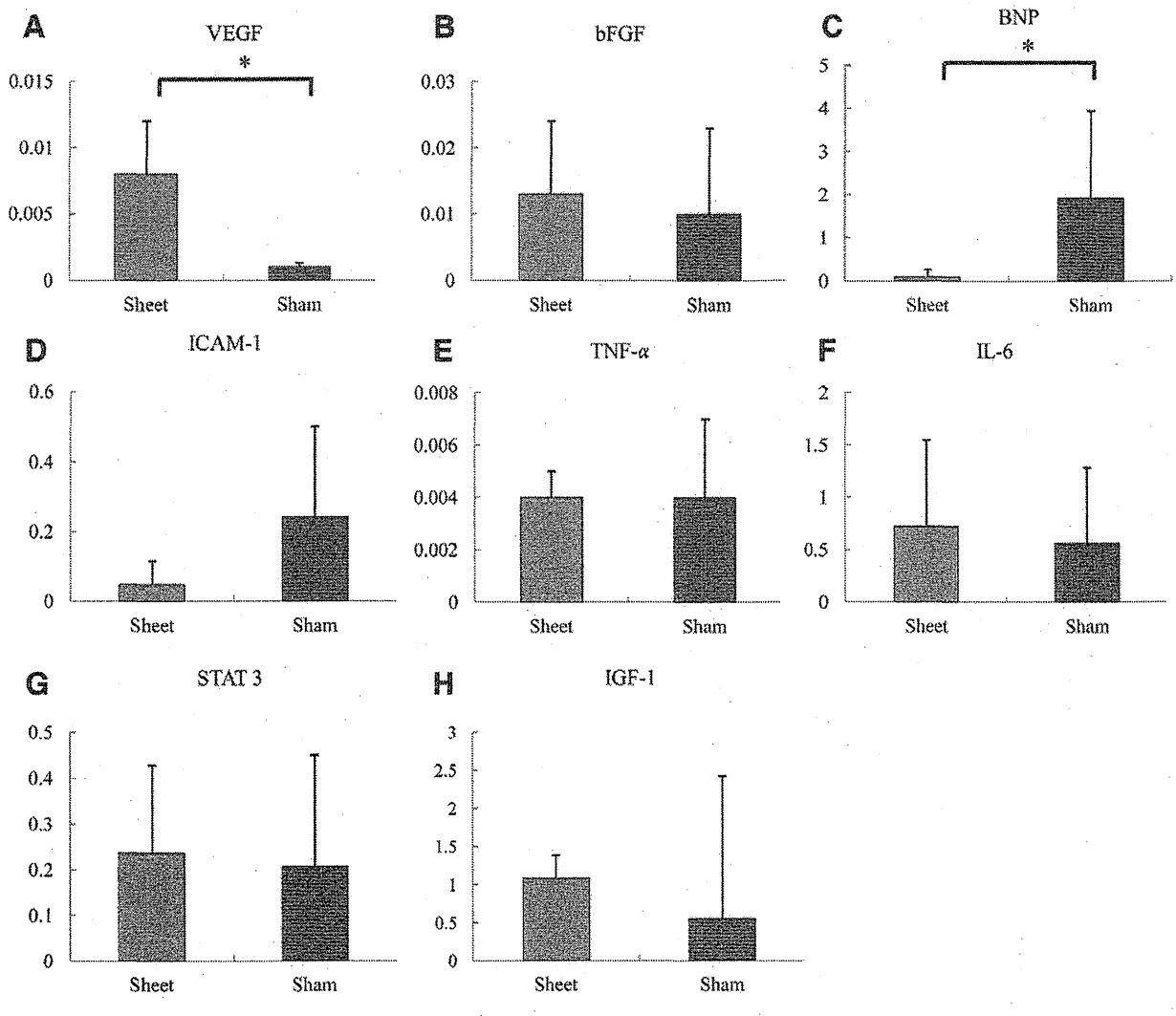

Figure 6. mRNA expression in cell-sheet implanted infarcted hearts determined by real-time PCR using porcine primers (**A–H**). VEGF mRNA expression was significantly increased in the Sheet group as compared with the Sham group. n=6 in each group; *P<0.05. PCR, polymerase chain reaction; VEGF, vascular endothelial growth factor.

after the treatment, both LVEDV and LVESV were significantly smaller and LVEF still greater in the Sheet group than in the Sham operation group (**Figure 3, Table**).

Myocardial Layer-Specific Recovery

Regional LV function in the infarct, border and remote areas was also examined in a myocardial-layer specific manner to assess the regional effects of SMB cell-sheet implantation in more detail by using the TMSP at 4 and 8 weeks post cell-sheet implantation (**Figure 4, Table**). Before the treatment, myocardial strain values of both the subendocardium and subepicardium were significantly smaller in the infarct and border areas compared with the remote area. After the sham operation, myocardial strain in both the subendocardium and subepicardium showed similar values for the infarct, border, and remote areas for 8 weeks. In contrast, subendocardial strain significantly increased at 4 and 8 weeks after cell-sheet implantation and was significantly larger than subepicardial strain in the treated border region. In the infarcted region, both subendocardial and subepicardial strain values tended to be greater in the Sheet group than in the Sham group. In the remote region, no significant changes were observed.

Modulation of Myocardial Structure

Myocardial structure, including fibrosis and vascularity, was assessed by HE staining, Masson's trichrome staining and immunohistochemistry for vWF at 8 weeks after the treatment (**Figures 5A,B**). The LV cavity was enlarged after the sham operation compared with after sheet implantation, and myocardial structure was well maintained post-sheet implantation compared with post-sham operation, as assessed by HE staining. Collagen had densely accumulated in the infarct area and was globally distributed in the remote area post-sham operation, whereas less collagen accumulated in either the infarct or remote area post-cell-sheet implantation compared with post-sham operation, as assessed by Masson's trichrome staining. The size of the infarcted area (ie, the percentage calculated as the positively stained LV area/total LV area), quantitatively